The thalamus drives light-evoked activity in the habenula of larval zebrafish

◆Ruey-Kuang Cheng[1], ◆Seetha Krishnan[2], Qian Lin[2], David G. C. Hildebrand[3, 4], Isaac H. Bianco[4] and *Suresh Jesuthasan[1, 5, 6, 7]

[1]Lee Kong Chian School of Medicine, Nanyang Technological University, Singapore 636921.

[2]NUS Graduate School for Integrative Sciences and Engineering, 28 Medical Drive, National University of Singapore, Singapore 117456.

[3]Graduate Program in Neuroscience, Division of Medical Sciences, Graduate School of Arts and Sciences, Harvard University, Cambridge, Massachusetts 02138 United States of America.

[4]Department of Molecular and Cell Biology, Harvard University, Cambridge, Massachusetts 02138, United States of America.

[5]Neural Circuitry and Behavior Laboratory, Institute of Molecular and Cell Biology, Singapore 138673.

[6]Neuroscience and Behavioral Disorders Program, Duke-NUS Graduate Medical School, 8 College Road, Singapore 169857.

[7]Department of Physiology, National University of Singapore, Singapore 117597.

*Corresponding author: sureshj@ntu.edu.sg; +65 65869545

◆equal contribution

Abstract

The habenula integrates sensory stimuli and reward information to regulate the release of neuromodulators with broad effects on brain state and behavior. One stimulus that affects habenula activity is light, but how it does so is unknown. Here, we address this question using larval zebrafish. Calcium imaging shows that light evokes widespread activity in habenula neurons, coupled with a prominent early response in the dorsal left neuropil. Injection of a lipophilic dye into this region retrogradely labels a retino-recipient thalamic nucleus. Anterograde tracing of the thalamus demonstrates a projection to the habenula, while optogenetic and lesion experiments confirm functional connectivity. An analysis of the mouse mesoscale connectome indicates that a visual nucleus in the thalamus, the ventral lateral geniculate nucleus, projects to the habenula in this species also. Together, these data suggest the existence of a conserved thalamo-habenula projection that enables light to affect habenula activity in vertebrates.

Introduction

The habenula is an evolutionarily conserved structure (Stephenson-Jones et al., 2012) that influences multiple behaviors, ranging from fear (Agetsuma et al., 2010; Lee et al., 2010; Zhang et al., 2016), to learning (Matsumoto and Hikosaka, 2007; 2009; Amo et al., 2014), addiction (Fowler et al., 2011), sleep (Aizawa et al., 2013), aggression (Chou et al., 2016; Golden et al., 2016) and performance under stress (Thornton and Davies, 1991). It acts by regulating the release of broadly-acting neuromodulators such as serotonin, dopamine, epinephrine and histamine (Wang and Aghajanian, 1977; Morley et al., 1985; Jhou et al., 2009; Quina et al., 2014). To precisely control these neuromodulators, such that behavior is appropriate for a given context, the habenula integrates diverse information including internal state, sensory stimuli and reward value.

These different types of information reach the habenula via different pathways. Internal states such as the circadian clock may be conveyed from the hypothalamus, for example by hypocretin-secreting neurons (Appelbaum et al., 2009). Negative reward causes the entopeduncular nucleus, or internal segment of the globus pallidus, to send excitatory input to the habenula (Hong and Hikosaka, 2008). Sensory stimuli such as odours evoke activity in the zebrafish habenula (Dreosti et al., 2014; Krishnan et al., 2014) via a direct pathway from the olfactory bulb (Miyasaka et al., 2009). Another stimulus that causes activity in the habenula is light, as has been demonstrated in rat (Zhao and Rusak, 2005), pigeon (Semm and Demaine, 1984) and zebrafish (Dreosti et al., 2014). How light affects the habenula is not known, implying the existence of an input pathway that is not yet well defined.

The habenula is divided into two major regions based on pattern of connectivity. In mammals, these are called the medial and lateral habenula, while in fish these are the dorsal and ventral habenula. In larval zebrafish, short pulses of red light cause asymmetric depolarization of the dorsal habenula, with more cells in the left side showing response; the response in the ventral habenula is symmetric (Dreosti et al., 2014). This response is dependent on the eyes (Dreosti et al., 2014), but no direct pathway from the retina to the habenula has been documented (Burrill and Easter, 1994; Robles et al., 2014). By retrograde tracing in adult zebrafish, Turner et al (Turner et al., 2016) proposed that the habenula receives input from the nucleus rostrolateralis, a thalamic nucleus with retinal input that is found in fish (Butler and Saidel, 2003; Saidel, 2013). However, no connectivity with the retina was shown, and because the thalamic nucleus does not asymmetrically innervate the left habenula and potential artifacts in labeling, the source of light-evoked activity in the habenula could not be determined (Turner et al., 2016). Here, using a combination of imaging, tracing and manipulation, we

demonstrate that light-evoked activity in the habenula of zebrafish larva is mediated by a thalamic nucleus with retinal input, i.e. the putative nucleus rostrolateralis. We then ask whether a similar pathway could exist in mammals.

Results

The habenula displays a broad and dynamic response to irradiance change

The zebrafish habenula consists of neurons surrounding neuropils that are innervated by afferent neurons (Hendricks and Jesuthasan, 2007; Miyasaka et al., 2009; Amo et al., 2014; Turner et al., 2016). To gain insight into the neural circuits that enable light to influence the habenula, we first characterized habenula activity evoked by pulses of light. Two-photon imaging was performed on a transgenic zebrafish line expressing the calcium indicator GCaMP3 throughout the habenula (Krishnan et al., 2014) (Figure 1A). Resonant-scanning, combined with piezo-driven focusing, was used to record the activity of cells at multiple focal planes (Figure 1B, C). With a step size of 10 µm, so that each cell would be sampled only once, most of habenula could be covered with 5 planes at a rate of 1 Hz. Habenula activity was monitored as the larva was exposed to 20-second pulses of blue light. We used relatively long pulses, rather than brief flashes, to allow responses to transition as well as steady state to be identified. Pixel-wise analysis in one 7-day old fish indicates that evoked activity – both transient and sustained - occurred throughout the habenula in response to increase and decrease in irradiance and to light and darkness (Figure 1D, E). The spatio-temporal pattern of activity was reproducible across several cycles, as shown by the trajectory of the system through state space (Figure 1F).

To assess if these responses were reproducible across multiple fish, we imaged the habenula in 6 fish. Habenula neurons were segmented (Figure 2A-C; total of 4986

cells, with an average of 831 ± 53 cells (95% CI) per fish) and their activity was clustered by *k*-means. Cluster centers were classified by response type. Transient and sustained responses to increase and decrease in irradiance could be reliably evoked (Figure 2D-G). The mean percentage of responding cells per fish (±95% CI) were ON: 30.98 ± 9.94%; OFF: 19.03 ± 3.93%; Inhibitory: 7.93 ± 3.50%. Correlating the cells corresponding to the different response types revealed that, in general, neurons that were excited by an increase of irradiance did not fire to a decrease (Figure 2H, I). Some neurons that were inhibited by light did, however, show a response at light offset (Figure 2F, blue trace; see also Figure 1E, red trace). These observations confirm that the activity of zebrafish habenula neurons is affected by change in irradiance, and that in addition to excitation there is inhibition by light, as well as excitation to loss of light.

The s1011tGAL4 line drives GCaMP3 expression throughout the habenula, and the response in all focal planes imaged suggests that all domains of the habenula respond to change in light. To further test this, we imaged fish where specific domains could be identified. Using the narp promoter (Agetsuma et al., 2010) (Figure 3A-C), responses to light ON and OFF could be detected in the lateral subdomain of the dorsal habenula (dHbL) (Figure 3 D, G, H; n = 5 fish). As we lacked a driver that is specific for the medial subdomain of the dorsal habenula (dHbM), we assessed activity here by analyzing narp-negative regions of the dorsal habenula in *narp:GAL4, UAS:DsRed, elavl3:GCaMP6f* fish (Figure 3E, G, I; n = 5 fish). Additionally, we analyzed the interpeduncular nucleus (IPN), which receives input from all regions of the dorsal habenula (deCarvalho et al., 2014). Evoked activity was seen in all domains of the interpeduncular nucleus (Figure 3K, L), consistent with all domains of the dorsal habenula showing a response to change in irradiance. To assess the ventral habenula, we imaged a line with a calcium indicator under the control of the *dao* promoter (Amo et

al., 2014). Again, evoked activity was seen (Figure 3F, G, J; n = 8 fish). These results indicate that all domains of the habenula in larval zebrafish respond to change in illumination.

To further characterize light evoked activity, we used high speed widefield microscopy. With 200 Hz imaging, a strong and rapid increase in fluorescence was detected in a discrete region in the dorsal left habenula (Figure 4A-F; n = 6 fish), as well as bilaterally in the thalamic region, soon after the onset of visible light. Two-photon microscopy at 13 Hz suggests that the rapid increase in the habenula occurs in the dorsal left neuropil (Figure 4G-I; n = 4 fish). The increase suggests that there is asymmetric activation of the dorsal habenula by light, potentially caused by a stronger input to the dorsal left neuropil. The bilateral activation in the thalamic region argues against the habenula asymmetry being an artifact of asymmetric illumination or reporter expression.

Taken together, these results suggest that the habenula afferents providing information about illumination should have the following properties. Firstly, they should terminate broadly within the habenula. Secondly, there should be stronger activity at light onset in terminals innervating the dorsal left neuropil. Thirdly, they should respond to increase or decrease in irradiance. Fourthly, they should cause excitation and inhibition, and may thus include excitatory and inhibitory neurons

The thalamus provides input to the habenula

We next searched for afferents that could provide such properties in larval zebrafish. We focused initially on inputs that could account for the asymmetry in the dorsal habenula. The entopeduncular nucleus (EN) is the major source of habenula afferents in teleosts (Yañez and Anadon, 1994), including zebrafish (Amo et al., 2014;

Turner et al., 2016). This nucleus is labeled in the *Et(sqKR11)* line (Lee et al., 2010), providing a simple way of visualizing EN afferents to the habenula. Some labeled fibers were detected in the dorsal left neuropil, indicating that the EN does provide some innervation to this region of the habenula (Figure 5A). However, labeling in this neuropil was relatively sparse, compared with other neuropils. We therefore hypothesized that there may be other inputs, from an anatomically distinct population, that targets this neuropil. To test this, the lipophilic tracer DiD was injected into the dorsal left neuropil (n = 6 fish). In all cases, neurons in the dorsal left habenula (which extend dendrites into the neuropil), the parapineal, and a thalamic nucleus located ventrally to both habenula (Figure 5B-D) were labeled.

DiD label was not detected in any other regions of the brain, and only rarely in the entopeduncular nucleus, suggesting that the thalamus is the major source of input to the dorsal left neuropil. This is consistent with the early activity seen in the thalamus (Figure 4A-F). The label in the thalamus cannot represent anterograde label from the habenula, as tracing of projections from the habenula by expressing fluorescent proteins specifically in the habenula does not result in a projection to the thalamus (Movie 1). Moreover, the labeling of cell bodies in the thalamus (Figure 5D inset, E) indicates that this is likely to be a retrograde label. The neuropil of this thalamic nucleus contains terminals of retinal ganglion cells, as shown by DiI injection into the retina (Figure 5E). Thus, the habenula neuropil with a strong response to light is innervated by thalamic nuclei that receive retinal input. This is likely to be the nucleus rostrolateralis.

Expressing a fluorescent protein in thalamic neurons, using the *s1020tGAL4* driver (Figure 5F, G), led to label of terminals throughout the habenula (Movie 2). Thus, although the dorsal left neuropil receives input from the thalamus, the thalamus projection is not restricted to this region of the habenula.

The habenula may receive glutamatergic and GABAergic input from the thalamus

As noted above, light caused both increase and decrease in activity of habenula neurons, implying that there may be excitatory and inhibitory afferents. Using an antibody to vGlut1/2, glutamatergic pre-synapses were detected in all neuropils of the habenula (Figure 5H), indicating the existence of excitatory afferents. GAD65/67 labeled puncta could also be detected in habenula neuropils (Figure 5I). In the lateral regions, corresponding to the ventral habenula, labeled streaks were detected adjacent to cell bodies. These labels were not located within habenula neurons, as they did not co-localize with cytoplasmic label provided by GCaMP3, nor did they fill the cytoplasm, implying that these puncta and streaks must reside in habenula afferents (i.e. axon terminals) such as those labeled in Movie 2. Labeled cell bodies were seen below the level of the habenula (see Movie 3). Consistent with this, GABAergic neurons could be detected in the dorsal thalamus using the transgenic line *Tg(gad1b:RFP, vGlut2a:GAL4, UAS:eGFP)* (Satou et al., 2013) (Figure 5J, K; Movie 4). No label was seen in the entopeduncular nucleus, which has previously been shown to be glutamatergic (Amo et al., 2014; Turner et al., 2016). These observations confirm that the thalamus contains both glutamatergic and GABAergic neurons, as described previously (Mueller, 2012), which may mediate light-evoked excitation and inhibition of habenula neurons.

Optogenetic stimulation of the thalamus drives habenula activity

The lipophilic and transgenic tracing experiments documented in Figure 5 demonstrate anatomical connectivity from the thalamus to the habenula. To test functional connectivity, we used optogenetics. Channelrhodopsin-2 (ChR2) was expressed in thalamic neurons with the s1020tGAL4 driver (Fig. 6A). Experiments were carried out on fish lacking eyes, to prevent a response to visual stimulation. Short pulses

of blue light reproducibly caused an increase in fluorescence of GCaMP6f in habenula neurons of fish with expression of ChR2 in the thalamus (Figure 6B, D, G). Some response was seen in fish without ChR2 expression (Fig. 6F), suggesting that some habenula response may be due to non-ocular sensors such as deep brain photoreceptors (Matos-Cruz et al., 2011; Fernandes et al., 2013). The larger response in fish with ChR2 expression, however, suggests that there is functional connectivity between the thalamus and the habenula.

Irradiance change evokes activity in thalamus neurons

If the thalamus provides afferents mediating illumination-dependent activity in the habenula, thalamic neurons should respond to increase and decrease of illumination. To test this, calcium imaging was carried out in *s1020tGAL4, UAS:GCaMP6s* transgenic fish. A response to increase and decrease in illumination was detected in cell bodies in the anterior thalamus (Figure 7A-F) in all fish imaged (n = 5). Dendrites in the neuropil of the thalamus also responded to change in illumination. Increase in irradiance caused activity more dorsally, while decrease caused activity more ventrally (Figure 7G-J). Thus, the thalamus has a response to both increase and decrease of illumination.

Habenula response to light has been shown to depend on the eyes (Dreosti et al., 2014). Thus, if the thalamus mediates habenula response to light, light-evoked activity here should depend on the eyes. Indeed, the robust responses to light were lost in fish lacking eyes (Figure 7K-S), consistent with this hypothesis.

Functional asymmetry in light-evoked activity

As shown in Figure 4G-I, light evokes strong activity in the dorsal neuropil of the left habenula. As the line used in this imaging experiment contains only labelled

habenula neurons, the response probabaly occur in dendrites. Given that there is no obvious anatomical asymmetry in thalamic input to the habenula (Figure 5F, G; see also Turner et al, 2016), we hypothesized that there may be functional asymmetry in activity within thalamic inputs. To test this, we imaged the terminals of thalamic axons using *s1020tGAL4, UAS:GCaMP6s* fish. Thalamic terminals in the dorsal left neropil showed a greater activity compared to those in the right neuropil (Figure 8). Thus, preferential light-evoked activity in thalamic afferents that project to the dorsal left neuropil may underlie the asymmetric dorsal habenula response.

Thalamic lesion inhibits habenula response to illumination change

To further test if the thalamus contributes to light evoked activity in the habenula, we lesioned the thalamic neuropil with a two-photon laser. This technique is expected to injure fibers innervating the neuropil (Semmelhack et al., 2014). The laser was targeted to the neuropil of the putative nucleus rostrolateralis, which was identified by first imaging the response to light pulses (Figure 9A, B). Lesioning led visible damage in the neuropil (Figure 9D), and to a reduction of evoked activity in the thalamus and habenula (Figure 9C, E-G, I, L, M). There was some variability in the effect (Figure 9N), possibly reflecting the limitations of this technique in enabling consistent ablation. Lesioning other targets of retinal ganglion cell axons, which are located more posteriorly, did not lead to a loss of light-evoked activity in the habenula (Figure 9G, I, J, K), indicating that this technique did not cause indiscriminate damage. These observations support the hypothesis that the putative nucleus rostrolateralis of the thalamus has a role in light-evoked activity in the habenula of larval zebrafish.

A thalamo-habenula projection in the mouse

Finally, we asked whether a projection from the thalamus to the habenula,

239 especially from a visual nucleus, is restricted to zebrafish, or whether it could also exist
240 in a mammal. To do this, we examined the mouse mesoscale connectome (Oh et al.,
241 2014). A search of the connectivity database derived from AAV injections into p56 mice,
242 using thalamus as the injection site and epithalamus as the target site, yielded 18 hits
243 covering different thalamic nuclei. Three experiments (numbers 267538006, 525796603
244 and 147212977) had been targeted to the ventral lateral geniculate nucleus. In one case
245 (Figure 10), the anterograde tracer virus had been injected into a Slc32a1-IRES-Cre
246 mouse, which expresses Cre in GABAergic neurons. Viral tracing in the mouse thus
247 suggests that a visual nucleus in the thalamus projects to the habenula in a mammal.

248 Discussion

249 We have investigated how illumination conditions influence activity in the habenula
250 of larval zebrafish. The pineal, although light responsive, does not innervate the
251 zebrafish habenula (Yáñez et al., 2009) while the parapineal, which innervates the
252 habenula, has been shown to be dispensable (Dreosti et al., 2014). Calcium imaging
253 suggests that the afferent neurons mediating responses to light should terminate broadly
254 in the habenula, cause stronger activity in the dorsal left neuropil, depolarize to increase
255 or decrease in irradiance, and potentially include excitatory and inhibitory neurons.
256 Several observations suggest that afferent neurons with these properties reside in the
257 thalamus.

258 Lipophilic tracing of the habenula and transgenic labeling of thalamic neurons
259 demonstrate that the thalamus directly innervates the larval zebrafish habenula. High-
260 speed imaging with widefield microscopy suggests that there is correlated activity in the
261 thalamus and habenula, consistent with functional connectivity. Although widefield
262 imaging uses visible light to excite the reporter, the rate of imaging used here is faster
263 than the rise time of GCaMP6f (Chen et al., 2013), so initial images reflect activity prior

to onset of the stimulating light. Further evidence for functional connectivity is provided by optogenetic stimulation of the thalamus, which causes a response in the habenula. Moreover, lesion of the thalamus reduced light-evoked activity in the habenula. The thalamus responds to both increase and decrease in illumination, and contains both excitatory and inhibitory neurons; no other source of GABAergic inputs to the zebrafish habenula has been described. Thus, by optical recording, anatomical tracing, activation and lesion, our data suggests that the thalamus mediates the habenula responses to irradiance change in larval zebrafish.

The region of the thalamus mediating activity in the habenula appears to be the nucleus rostrolateralis, as proposed by Turner et al (2016). The neuropil here can be functionally separated into two domains, based on the response to light – excitation to light OFF in the ventral regions and excitation to light ON more dorsally. This neuropil contains two previously defined targets of retinal ganglion cells, AF2 and AF4 (Burrill and Easter, 1994). AF4 is innervated predominantly by M3 and M4 retinal ganglion cells (Robles et al., 2014), which extend their dendritic tree into the proximal layer of the inner plexiform layer and are considered ON neurons. AF2 is innervated by B1 retinal ganglion cells that have dendrites in the distal layer (Robles et al., 2014), and these may account for the OFF responses in the thalamus and habenula. This thalamic nucleus may also receive input from non-retinal sources, but this remains to be investigated. The loss of a thalamic response to light in fish lacking eyes, however, suggests that such contribution may be minor.

Light is a potent regulator of brain function. It can affect mood (Vandewalle et al., 2010), alertness (Badia et al., 1991), cognitive ability (LeGates et al., 2012) and movement (Aschoff, 1960; Burgess and Granato, 2007). These phenomena are sensitive to irradiance, not image formation, and are mediated by a number of sensors

289 including intrinsically-sensitive retinal ganglion cells whose targets include the thalamus
290 (Hattar et al., 2006). The ability of light to affect normal movement patterns (Burgess et
291 al., 2010) or to disrupt mood and cognition (LeGates et al., 2012) involves
292 neuromodulators such as serotonin, and changing irradiance affects activity in the dorsal
293 raphe (Fite et al., 2005; Cheng et al., 2016). Based on the data here, and the well-
294 established roles of the habenula in regulating neuromodulators, we suggest that some
295 of these effects of light may be mediated by the thalamic projection to the habenula.

296 A projection from the thalamus to the habenula may be evolutionarily conserved in
297 vertebrates. In humans and rabbits, a thalamo-habenula projection was proposed many
298 years ago based on degeneration experiments (Marburg, 1944; Cragg, 1961). Using
299 retrograde tracing with horseradish peroxidase, a projection from the dorsal thalamus to
300 the habenula was reported in a lizard (Díaz and Puelles, 1992). Hints of a projection can
301 also be seen in a tracing experiment performed in rats (Moore et al., 2000). The large-
302 scale mouse mesoscale connectome project (Oh et al., 2014), which uses viral-based
303 anterograde tracing, provides the most recent evidence for a thalamo-habenula
304 projection in a mammal. This technique suggests a projection from the ventral lateral
305 geniculate nucleus and other thalamic nuclei to the habenula. It will be interesting to
306 determine whether a similar anatomical connection exists in humans, as this may
307 contribute to the high functional connectivity between the thalamus and habenula
308 reported recently (Torrisi et al., 2016).

309 ## Materials and Methods

310 ### Fish lines

311 Experiments were performed in accordance with guidelines issued by the
312 Institutional Animal Care and Use Committee of the Biological Resource Centre at

Biopolis, Singapore. Zebrafish (*Danio rerio*) lines used for this study were: *Tg(UAS:GCaMP6s)sq202*, SqKR11Et, *GAL4s1011t*, *GAL4s1020t,* Tg(UAS:GCaMP3)sq200, *Tg(elavl3:GCaMP6f)a12200*, *Tg(UAS:ChR2-eYFP)* (Arrenberg et al., 2009) and AB wildtype.

Tg(elavl3:GCaMP6f)a12200 was generated by PCR amplification of the GCaMP6f open reading frame (Addgene plasmid 40755 (Chen et al., 2013)) with forward primer ataACTAGTgccaccATGGGTTCTCATCATCAT and reverse ataCCGCGGcTCACTTCGCTGTCATCATTTGTAC (restriction site and coding sequences are in upper case). This fragment was cloned into a plasmid with Tol2 arms flanking an upstream attR1-R2 cassette and the insertion site using restriction enzymes SpeI and SacII. Previously described *elavl3* (*HuC*) *cis*-regulatory elements (Higashijima et al., 2003) were placed upstream via LR recombination (Invitrogen) with an attL flanked *elavl3* entry clone. The resulting plasmid was then co-injected into 1-cell stage embryos at a concentration of 30 ng/µL with Tol2 transposase mRNA at a concentration of 30 ng/µL. A single founder was selected based on high and spatially broad expression. Outcrossing this founder generated 50% GCaMP6f-positive embryos, which were selected to establish the line.

Imaging

Zebrafish larvae (aged 5 - 10 dpf) were anaesthetized in mivacurium and embedded in low-melting temperature agarose (1.2-2.0 % in E3) in a glass-bottom dish (Mat Tek). They were imaged on a Nikon two-photon microscope (A1RMP), attached to a fixed stage upright microscope, using a 25x water immersion objective (NA = 1.1). The femtosecond laser (Coherent Vision II) was tuned to 920 nm for GCaMP imaging. Stacks were collected in resonant-scanning mode with a 525/50 nm bandpass emission filter

and with 8x pixel averaging; single-plane images were collected in galvano-scanning mode with 2x pixel averaging. The sample size was based on (Dreosti et al., 2014).

Light stimuli were generated by 5 mm blue LEDs (458 nm peak emission). They were powered by a 5 V TTL signal from a control computer and synchronized with image capture using a National Instruments DAQ board, controlled by the Nikon Elements software. Light intensity at the sample was 0.13 mW/cm^2.

For widefield microscopy, excitation was provided by LEDs (Cairn OptoLED) at 470 nm. Images were captured on a Zeiss Axio Examiner with a 20x water immersion objective, using a Flash4 camera (Hamamatsu) controlled by MetaMorph. After background subtraction, change in fluorescence was measured using the deltaF-up command in Fiji.

Data analysis

Initial Data Preprocessing: Raw images obtained were first registered to correct for any vertical/horizontal movement artifacts using cross correlation. Then, a median filter of size 3 was applied to remove noise. A darker region outside the region of interest was chosen as the background and subtracted from the image to remove any background noise. Non linear trends in the data were detrended using polynomials of order 2-5. Data was then normalized into Z-scores by subtracting the overall mean and dividing by the standard deviation. A rolling window average was then used to smooth noisy traces where necessary. Where possible, cells were segmented or images were directly analysed as pixels (see Below).

Correlation to light evoked activity: Temporal traces from pixels (Thalamus or Thalamic afferents) or segmented cells (in the habenula) were classified as responding

to light ON or OFF by calculating their correlation coefficient to a square wave that is 1 when the light is ON or when light is OFF and 0 during other time periods. High correlation to these traces indicated that the pixel or cell is responding to light ON or OFF respectively.

Pixel based analysis of the habenula and thalamus: To show the spatial and temporal distribution of light evoked activity in the habenula and thalamus, the Thunder platform (Freeman et al., 2014) was used for fast pixel based clustering and factorization.

PCA: Principal Component Analysis (PCA) was used to obtain a low dimensional representation of the population. In normal fish, in the habenula (Figure 1D) and thalamus (Figure 7M), the first two Principal Components (PC) easily picked up the evoked responses to light ON and OFF. The explained variance, though small, decayed rapidly after the first component (Figure 1D, variance explained PC1 12.92%, PC2 6.12% and PC3 4.57%; first 20 PCs 55.60% ; Figure 7M, variance explained PC1 11.87%, PC2 3.61% and PC3 2.67%; first 20 PCs 40.82%) and hence the first two PCs were chosen to plot the data in low dimension. They showed reproducible state changes in the population to changes in irradiance. In eye lesioned fish (Figure 7P) however, neither of the first twenty PCs (variance explained PC1 4.92%, PC2 4.24% and PC3 3.26%; first 20 PCs 39.53%) showed any discernable correlation to light evoked activity (The inset in Figure 7P). The first two are plotted in Figure 7P for comparison with controls. Correlation coefficients plotted in insets of Figure 7M and 7P were obtained by correlating the PCs with a trace that was 1 when light was ON and 0 otherwise.

K-means: K-means clustering was performed to identify pixels with similar responses profiles. Given the uncertainty of k-means to the optimal cluster number, an iterative approach was used to separate pixels relating to evoked responses versus

pixels that don't (here referred to as noise clusters). The number of clusters were chosen to reveal as many stimulus related clusters as possible, until there was little change in the number and types of stimulus related clusters and increase in noise related clusters. Noise clusters were then removed from the spatial and temporal plots for clarity. It is to be noted that this analysis does have its drawbacks when used to analyse data with variable variance and cannot not capture all possible types of responses. Multiple runs were made to ensure that noisy pixels were not clustered into evoked clusters. Where applicable cell segmentation and manual classification was used. For example, we were not able to separate inhibitory clusters from off custers in Figure 3E-G. This was revealed when the cells were segmented, and their temporal traces inspected. In all cases, K-means cluster center showing evoked responses to light ON were colored in shades of blue and those showing responses to light OFF were colored in shades of red. Pixels belonging to the cluster were colored similarly and superimposed on an average image of the plane analysed. In different datasets, on average, this analysis provided an optimal k of 6-10; 3-4 clusters that didn't correspond to evoked activity were not included while plotting.

For data following eye lesion (FIgure 7) and thalamic neuropil/AF9/AF7 lesion (Figure 9), k-means was performed to differentiate responses between the controls and the lesion. Hence, number of clusters were chosen such that cluster center adequately differentiated responses before and after lesion. Cluster center not responding to light were also plotted here. To verify the results of k-means, the presence of light response was verified by examining the pixels (Figure 8 Q-S) or segmenting the cells (Figure 9 J-N) in both control and lesioned animals.

The scripts used for analysis are provided at http://dx.doi.org/10.5061/dryad.q0171.

Cell segmentation: Each stack was scaled 2x in imageJ, then maximally projected to a single image, which was then subjected to a minimum filter and unsharp mask to sharpen the boundary of cells. ROIs were identified using the "find maxima…" command, as a way to localize regional darkest point as the center of each ROI. The boundary of the ROI was outlined by "analyze particle…" that connects bright pixels into mosaic-like tessellated plane, encircling each darkest point. Each ROI was then numbered sequentially using the ImageJ ROI Manager and mapped back to the original despeckled image stack. Manual segmentation was done here to delete extraneous ROIs outside the habenula and to encircle cells that were not detected by the algorithm (<10% of total ROIs). In the last step, "Set measurements…" and "measure" in ImageJ provided the mean fluorescence value of all pixels within each ROI across the entire image stack and the x-y coordinates of each ROI. Time-lapse series in which z drifting occurred were excluded, as in this case ROIs could not be defined.

K-means on segmented cells: For Figures 2D-F, *k-means* was performed from cells segmented by the semi automated algorithm described above. The purpose is to determine heterogeneity of temporal responses to changes in irradiance, accurately classify cells into ON, OFF and Inhibitory responses and perform correlation between them. Analysis was done on traces from 4986 habenula cells from 6 fish. Traces were detrended, smoothed and normalized to z-scores using baseline as the time before the first blue light. Traces that did not reach a Z-score of 2 during the period of irradiance change were classified as not having an evoked response and not included in the clustering analysis. 2456 of 4986 cells were thus removed. *K-means* was first run with an arbitrary k = 60. This generated a wide range of clusters capturing the temporal heterogeneity of the responses. The clusters were then divided into ON, OFF, Inhibitory and no evoked response. Neurons belonging to each cluster were correlated among

each other and to the cluster center. If they had an evoked response, they were correlated with other clusters and assigned to one with the highest correlation. Otherwise they were classified into the no evoked response category; 138 such cells were reclassified. Traces of cells belonging to ON, OFF and Inhibitory clusters are plotted as a heatmap in Figure 2G and their correlation coefficients in Figure 2H. Similarly, cells segmented from multiple fish were classified to reveal responses in different habenula regions as plotted in Figure 3H-J.

***Boxplots*:** Boxplots in Figures 7Q, 8D-E and 9N were plotted to show the full distribution of the data. The box in the boxplot ranges from the first quartile to the third quartile, and the box shows the interquartile range (IQR). The line across the box is the median of the data. The whiskers extend to 1.5*IQR on either side of the box. Anything above this range are defined as outliers and plotted as black diamonds in the plots.

Neural tracing

DiD (Life Technologies) was dissolved in 50 µl ethanol to make a saturated solution. This was heated to 55˚C for 5 minutes prior to injection into the fish that had been fixed in 4% paraformaldehyde. Fish were mounted in 1.2% low melting temperature agarose dissolved in PBS. The dye was pressure injected into the habenula under a compound microscope (Leica DM LFS), using a 20X water immersion objective. For labeling the retina, a saturated solution of DiI in chloroform was used. Injections were carried out under a stereo microscope (Zeiss Stemi 2000). After injections, fish were stored at 4˚C overnight to allow tracing, and then imaged with a 40x water immersion objective on a Zeiss LSM 710 confocal microscope.

Antibody label

Larvae were fixed in 4% para-formaldehyde/PBS overnight at 4˚C. They were then rinsed in PBS. The brains were dissected out, and permeabalized using 1% BSA (fraction V; Sigma), 0.1% DMSO and 0.1% Triton X-100. The antibodies used here, anti-vGlut1/2 (Synaptic Systems 135503, RRID:AB_1279466; 1:100) and anti-GAD65/67 (Abcam ab11070, RRID:AB_297722; 1:500), have previously been used in zebrafish (Wyart et al., 2009; Lee et al., 2010). The brains were incubated in the primary antibody overnight, rinsed several times in PBS, then incubated in secondary antibody (Alexa 488 goat anti-rabbit; 1:1000). After washing, these were mounted in 1.2% agarose/PBS. Imaging was carried out using a Zeiss LSM 510 laser scanning confocal microscope, with a 40x water immersion objective.

Optogenetic stimulation

5 dpf *Tg(s1020GAL4, UAS:ChR2-eYFP, elavl3:GCaMP6f)* larvae were used. The eyes were removed using fine tungsten needles in fish that were anesthetized with MS222. This procedure was carried out in Ringers saline. Fish were then mounted in 1.2% agarose in Ringers saline, and imaged using two-photon microscopy as described above, at 1 Hz. Optical stimulation was carried out using a 50 µm fiber optic probe (Doric Lenses), placed approximately 20 µm from the thalamus. The 465 nm LED (Doric) was driven with a current of 900 mA, 30 seconds after the start of imaging. 10 pulses were provided, with a pulse duration of 25 milliseconds and a frequency between 1 and 8 Hz. Each fish was exposed to at least 3 pulse trains. For Figure 6B-C, the average of the first 29 frames was used as a reference. The ratio of all frames relative to this reference was obtained using FIJI. The analysis to generate Figure 6G was blind to the genotype.

Enucleation

5 day-old fish were anaesthetized in Ringer's saline containing MS222. The eyes were removed using electrolytically sharpened tungsten needles. Fish were allowed to recover for several hours in anesthetic-free saline. Activity recorded 2 - 4 hours after eye removal. To enable lateral imaging of the thalamus (Figure 7H-J), one eye was removed using this method.

Laser ablation

Tg(Elavl3:GCaMP6f) larvae were anaesthetized and then mounted in 2% low-melting temperature agarose. Lesions were created with the femto-second laser tuned to 960 nm and fixed on a single point. Several pulses, each lasting 100 - 500 msec, were used. Lesioning was monitored by time-lapse imaging before and after each pulse, and was terminated when there was a localized increase in GCaMP6f fluorescence. The formation of a bubble indicates that lesioning involved plasma formation (Venugopalan et al., 2002). These can be imaged in the red channel of the two-photon microscope. Sample size was chosen based on (Aizenberg and Schuman, 2011). Animals with bleeding in the brain after lesioning, due to bursting of a blood vessel in the thalamis, were discarded.

Analysis of the mouse mesoscale connectome

The mouse connectivity atlas (http://connectivity.brain-map.org/) was searched in ""Target Search" mode, using "TH" as the source structure and "EPI" as the target structure. The minimum target volume listed was 0.005 mm^3. For each hit, serial transverse sections containing the habenula, which had been imaged by two-photon microscopy, were screened manually to verify that there were labelled fibers within the

habenula.

Acknowledgements

This work was funded by core funding from the Institute of Molecular and Cell Biology and a grant from the Ministry of Education, Singapore. SK and QL were supported by fellowships from the National University of Singapore. DGCH was supported by NIH grant 5T32HL007901. We thank Caroline Kibat for technical assistance and Claire Wyart for providing the *UAS:ChR2-eYFP* transgenic line.

Author contributions

Experiments were designed by CRK, QL and SJ. CRK carried out two-photon imaging. SK developed software and analyzed imaging data. DGCH and IHB generated the *elavl3:GCaMP6f* transgenic line. SJ performed wide-field imaging, analysis, dye tracing, optogenetic manipulation and wrote the manuscript.

References

Agetsuma M, Aizawa H, Aoki T, Nakayama R, Takahoko M, Goto M, Sassa T, Amo R, Shiraki T, Kawakami K, Hosoya T, Higashijima S-I, Okamoto H (2010) The habenula is crucial for experience-dependent modification of fear responses in zebrafish. Nat Neurosci 13:1354–1356.

Aizawa H, Yanagihara S, Kobayashi M, Niisato K, Takekawa T, Harukuni R, McHugh TJ, Fukai T, Isomura Y, Okamoto H (2013) The synchronous activity of lateral habenular neurons is essential for regulating hippocampal theta oscillation. J Neurosci 33:8909–8921.

Aizenberg M, Schuman EM (2011) Cerebellar-Dependent Learning in Larval Zebrafish. J Neurosci 31:8708–8712.

524 Amo R et al. (2014) The habenulo-raphe serotonergic circuit encodes an aversive
525 expectation value essential for adaptive active avoidance of danger. Neuron
526 84:1034–1048.

527 Appelbaum L, Wang GX, Maro GS, Mori R, Tovin A, Marin W, Yokogawa T, Kawakami K,
528 Smith SJ, Gothilf Y, Mignot E, Mourrain P (2009) Sleep-wake regulation and
529 hypocretin-melatonin interaction in zebrafish. Proceedings of the National Academy
530 of Sciences 106:21942–21947.

531 Arrenberg A, Arrenberg AB, Del Bene F, Del Bene F, Baier H, Baier H (2009) Optical
532 control of zebrafish behavior with halorhodopsin. Proceedings of the National
533 Academy of Sciences 106:17968–17973.

534 Aschoff J (1960) Exogenous and endogenous components in circadian rhythms. Cold
535 Spring Harb Symp Quant Biol 25:11–28.

536 Badia P, Myers B, Boecker M, Culpepper J, Harsh JR (1991) Bright light effects on body
537 temperature, alertness, EEG and behavior. Physiol Behav 50:583–588.

538 Burgess HA, Granato M (2007) Modulation of locomotor activity in larval zebrafish during
539 light adaptation. J Exp Biol 210:2526–2539.

540 Burgess HA, Schoch H, Granato M (2010) Distinct retinal pathways drive spatial
541 orientation behaviors in zebrafish navigation. Curr Biol 20:381–386.

542 Burrill JD, Easter SS (1994) Development of the retinofugal projections in the embryonic
543 and larval zebrafish (Brachydanio rerio). J Comp Neurol 346:583–600.

544 Butler AB, Saidel WM (2003) Clustered phylogenetic distribution of nucleus
545 rostrolateralis among ray-finned fishes. Brain Behav Evol 62:152–167.

546 Chen T-W, Wardill TJ, Sun Y, Pulver SR, Renninger SL, Baohan A, Schreiter ER, Kerr
547 RA, Orger MB, Jayaraman V, Looger LL, Svoboda K, Kim DS (2013) Ultrasensitive
548 fluorescent proteins for imaging neuronal activity. Nature 499:295–300.

549 Cheng R-K, Krishnan S, Jesuthasan S (2016) Activation and inhibition of tph2
550 serotonergic neurons operate in tandem to influence larval zebrafish preference for
551 light over darkness. Sci Rep 6:20788.

552 Chou M-Y, Amo R, Kinoshita M, Cherng B-W, Shimazaki H, Agetsuma M, Shiraki T, Aoki
553 T, Takahoko M, Yamazaki M, Higashijima S-I, Okamoto H (2016) Social conflict
554 resolution regulated by two dorsal habenular subregions in zebrafish. Science
555 352:87–90.

556 Cragg BG (1961) The connections of the habenula in the rabbit. Exp Neurol 3:388–409.

557 deCarvalho TN, Subedi A, Rock J, Harfe BD, Thisse C, Thisse B, Halpern ME, Hong E
558 (2014) Neurotransmitter map of the asymmetric dorsal habenular nuclei of zebrafish.
559 Genesis 52:636–655.

560 Díaz C, Puelles L (1992) Afferent connections of the habenular complex in the lizard
561 Gallotia galloti. Brain Behav Evol.

562 Dreosti E, Vendrell-Llopis N, Carl M, Yaksi E, Wilson SW (2014) Left-right asymmetry is
563 required for the habenulae to respond to both visual and olfactory stimuli. Curr Biol
564 24:440–445.

565 Fernandes AM, Fero K, Driever W, Burgess HA (2013) Enlightening the brain: Linking
566 deep brain photoreception with behavior and physiology. Bioessays 35:775–779.

567 Fite KV, Wu PS, Bellemer A (2005) Photostimulation alters c-Fos expression in the

568 dorsal raphe nucleus. Brain Res 1031:245–252.

569 Fowler CD, Lu Q, Johnson PM, Marks MJ, Kenny PJ (2011) Habenular α5 nicotinic
570 receptor subunit signalling controls nicotine intake. Nature 471:597–601.

571 Golden SA et al. (2016) Basal forebrain projections to the lateral habenula modulate
572 aggression reward. Nature 534:688–692.

573 Hattar S, Kumar M, Park A, Tong P, Tung J, Yau K-W, Berson DM (2006) Central
574 projections of melanopsin-expressing retinal ganglion cells in the mouse. J Comp
575 Neurol 497:326–349.

576 Hendricks M, Jesuthasan S (2007) Asymmetric innervation of the habenula in zebrafish.
577 J Comp Neurol 502:611–619.

578 Higashijima S-I, Masino MA, Mandel G, Fetcho JR (2003) Imaging neuronal activity
579 during zebrafish behavior with a genetically encoded calcium indicator. J
580 Neurophysiol 90:3986–3997.

581 Hong S, Hikosaka O (2008) The globus pallidus sends reward-related signals to the
582 lateral habenula. Neuron 60:720–729.

583 Jhou TC, Fields HL, Baxter MG, Saper CB, Holland PC (2009) The rostromedial
584 tegmental nucleus (RMTg), a GABAergic afferent to midbrain dopamine neurons,
585 encodes aversive stimuli and inhibits motor responses. Neuron 61:786–800.

586 Krishnan S, Mathuru AS, Kibat C, Rahman M, Lupton CE, Stewart J, Claridge-Chang A,
587 Yen S-C, Jesuthasan S (2014) The Right Dorsal Habenula Limits Attraction to an
588 Odor in Zebrafish. Curr Biol.

589 Lee A, Mathuru AS, Teh C, Kibat C, Korzh V, Penney TB, Jesuthasan S (2010) The
590 habenula prevents helpless behavior in larval zebrafish. Curr Biol 20:2211–2216.

591 LeGates TA, Altimus CM, Wang H, Lee H-K, Yang S, Zhao H, Kirkwood A, Weber ET,
592 Hattar S (2012) Aberrant light directly impairs mood and learning through
593 melanopsin-expressing neurons. Nature 491:594–598.

594 Marburg O (1944) The structure and fiber connections of the human habenula. Journal
595 of Comparative Neurology 80:211–233.

596 Matos-Cruz V, Blasic J, Nickle B, Robinson PR, Hattar S, Halpern ME (2011)
597 Unexpected diversity and photoperiod dependence of the zebrafish melanopsin
598 system. PLoS ONE 6:e25111.

599 Matsumoto M, Hikosaka O (2007) Lateral habenula as a source of negative reward
600 signals in dopamine neurons. Nature 447:1111–1115.

601 Matsumoto M, Hikosaka O (2009) Representation of negative motivational value in the
602 primate lateral habenula. Nat Neurosci 12:77–84.

603 Miyasaka N, Morimoto K, Tsubokawa T, Higashijima S-I, Okamoto H, Yoshihara Y
604 (2009) From the olfactory bulb to higher brain centers: genetic visualization of
605 secondary olfactory pathways in zebrafish. J Neurosci 29:4756–4767.

606 Moore RY, Weis R, Moga MM (2000) Efferent projections of the intergeniculate leaflet
607 and the ventral lateral geniculate nucleus in the rat. J Comp Neurol 420:398–418.

608 Morley BJ, Spangler KM, Javel E (1985) The development of somatostatin
609 immunoreactivity in the interpeduncular nucleus of the cat. Brain Res 352:241–248.

610 Mueller T (2012) What is the Thalamus in Zebrafish? Front Neurosci 6:64.

611 Oh SW et al. (2014) A mesoscale connectome of the mouse brain. Nature 508:207–214.

612 Quina LA, Tempest L, Ng L, Harris JA, Ferguson S, Jhou TC, Turner EE (2014) Efferent
613 Pathways of the Mouse Lateral Habenula. J Comp Neurol.

614 Robles E, Laurell E, Baier H (2014) The retinal projectome reveals brain-area-specific
615 visual representations generated by ganglion cell diversity. Curr Biol 24:2085–2096.

616 Saidel WM (2013) Nucleus Rostrolateralis: An Expansion of the Epithalamus in Some
617 Actinopterygii. The Anatomical Record 296:1594–1602.

618 Satou C, Kimura Y, Hirata H, Suster ML, Kawakami K, Higashijima S-I (2013)
619 Transgenic tools to characterize neuronal properties of discrete populations of
620 zebrafish neurons. Development 140:3927–3931.

621 Semm P, Demaine C (1984) Electrophysiology of the pigeon's habenular nuclei:
622 evidence for pineal connections and input from the visual system. Brain Res Bull
623 12:115–121.

624 Semmelhack JL, Donovan JC, Thiele TR, Kuehn E, Laurell E, Baier H (2014) A
625 dedicated visual pathway for prey detection in larval zebrafish. Elife 3:17968.

626 Stephenson-Jones M, Floros O, Robertson B, Grillner S (2012) Evolutionary
627 conservation of the habenular nuclei and their circuitry controlling the dopamine and
628 5-hydroxytryptophan (5-HT) systems. Proc Natl Acad Sci USA 109:E164–E173.

629 Thornton EW, Davies C (1991) A water-maze discrimination learning deficit in the rat
630 following lesion of the habenula. Physiol Behav 49:819–822.

631 Torrisi S, Nord CL, Balderston NL, Roiser JP, Grillon C, Ernst M (2016) Resting State
632 Connectivity of the Human Habenula at Ultra-High Field. Neuroimage:1–21.

633 Turner KJ, Hawkins TA, Yáñez J, Anadón R, Wilson SW, Folgueira M (2016) Afferent
634 Connectivity of the Zebrafish Habenulae. Front Neural Circuits 10:3512.

635 Vandewalle G, Schwartz S, Grandjean D, Wuillaume C, Balteau E, Degueldre C,
636 Schabus M, Phillips C, Luxen A, Dijk DJ, Maquet P (2010) Spectral quality of light
637 modulates emotional brain responses in humans. Proceedings of the National
638 Academy of Sciences 107:19549–19554.

639 Venugopalan V, Guerra A, Nahen K, Vogel A (2002) Role of Laser-Induced Plasma
640 Formation in Pulsed Cellular Microsurgery and Micromanipulation. Phys Rev Lett
641 88:078103.

642 Wang RY, Aghajanian GK (1977) Physiological evidence for habenula as major link
643 between forebrain and midbrain raphe. Science 197:89–91.

644 Wyart C, Del Bene F, Warp E, Scott EK, Trauner D, Baier H, Isacoff EY (2009)
645 Optogenetic dissection of a behavioural module in the vertebrate spinal cord. Nature
646 461:407–410.

647 Yáñez J, Busch J, Anadón R, Meissl H (2009) Pineal projections in the zebrafish (Danio
648 rerio): overlap with retinal and cerebellar projections. Neuroscience 164:1712–1720.

649 Yañez J, Anadon R (1994) Afferent and efferent connections of the habenula in the
650 larval sea lamprey (Petromyzon marinus L.): an experimental study. J Comp Neurol
651 345:148–160.

652 Zhang J, Tan L, Ren Y, Liang J, Lin R, Feng Q, Zhou J, Hu F, Ren J, Wei C, Yu T,

653 Zhuang Y, Bettler B, Wang F, Luo M (2016) Presynaptic Excitation via GABAB
654 Receptors in Habenula Cholinergic Neurons Regulates Fear Memory Expression.
655 Cell 166:716–728.

656 Zhao H, Rusak B (2005) Circadian firing-rate rhythms and light responses of rat
657 habenular nucleus neurons in vivo and in vitro. Neuroscience 132:519–528.

658 ## Figure legends

659 **Figure 1. The larval zebrafish habenula has a broad and complex response to**
660 **change in irradiance.** (A) Dorsal view of the head of a live 7 day-old fish, with GCaMP3
661 expression in the habenula (arrows) under the control of the *s1011t* GAL4 driver. (B) A
662 single two-photon slice through the dorsal habenula of the fish in panel A (boxed region).
663 (C) A yz reconstruction at the point indicated by the yellow line in panel B, showing a
664 transverse view of the habenula. The dotted lines indicate imaging planes separated by
665 10 µm. The yellow line indicates the plane imaged in B. Dashed lines show the border
666 of the habenula. (D) Spatial distribution of responses in the habenula of one fish (7 dpf)
667 to pulses of light. 5 planes are shown here. The colors are coded according to the
668 temporal pattern of response, as indicated in (E). Images were collected at a rate of 1
669 stack/second, and four pulses of light were delivered for 20 seconds each, with variable
670 inter-stimulus interval. (E) Centers of *k*-means clusters corresponding to colors of pixels
671 in (D). Cluster centers in (D) and the corresponding pixels in (E) indicating responses to
672 light ON are colored in shades of blue and light OFF in shades of red. The horizontal
673 black line represents Z-score of 0. (F) Trajectory of the habenula response in two-
674 dimensional state space, using the first two principal components (PC1 and PC2).
675 Traces are color-coded according to the wedges in panel E, to represent direction in
676 which change in irradiance drives the neural state. In panels E and F, the bold lines
677 correspond to light onset while the dashed lines indicate offset. The presence of light is

678 also indicated by the blue bars. lHb: left habenula; rHb: right habenula. a: anterior; p:
679 posterior. d: dorsal; v: ventral Scale bar = 100 µm in panel A, 25 µm elsewhere.

680 **Figure 2. Habenula response to irradiance change is reproducible.** (A-C)
681 Segmentation of habenula neurons using a semi-automated algorithm (see Methods).
682 (D-F) *K*-means cluster analysis of segmented habenula neuron responses to pulses of
683 blue light in 6 fish (7-8 dpf). Traces show cluster center, with shaded regions indicating
684 standard error of the mean. Clusters were grouped by their temporal activity pattern and
685 clusters with excitation to light ON (D) or OFF (E), or inhibition to light (Inhibitory, F) were
686 seen. Clusters without evoked responses are not shown. (G) Activity traces of each cell
687 from the 6 fish grouped into ON, OFF and Inhibitory (Inh) categories based on their
688 membership to the clusters shown in D-F. Horizontal black lines divide the categories.
689 (H) Correlation between activity of cells belonging to ON, OFF and Inhibitory (Inh)
690 clusters shown in D-F. In general, the ON and OFF responding cells were uncorrelated
691 (correlation coefficient < 0). Vertical and horizontal black lines divide ON, OFF and
692 Inhibitory categories. (I) Activity traces of cells in ON and OFF clusters that showed high
693 correlation with the other category (313 of 1767 cells). The traces showed that this
694 correlation may be due to OFF cells showing slow decay in fluorescence following light
695 ON. Manual inspection of the traces did not reveal any cells that responded reliably to
696 both light ON and OFF. Colorbar for panels G and I is shown below panel I. Scale bar =
697 25 µm.

698 **Figure 3. The response of different habenula subdomains to change in irradiance.**
699 (A-C) A *narp:GAL4, UAS:DsRed, Brn3a:eGFP* larva, with label in the dorsal habenula
700 (arrows) and projection to the IPN (arrowhead). A coronal (B) and reconstructed sagittal
701 (C) section through the left habenula, with dHbM in green and dHbL in magenta. (D)
702 Spatial distribution of responses in the dorsal habenula of a *narp:GAL4, UAS:GCaMP6s*

fish (8dpf). (E). Responses of non-DsRed cells in the dorsal habenula of a *elavl3:GCaMP6f, narp:GAL4, UAS:DsRed* fish (6dpf). (F) Responses in the ventral habenula of a *dao:GAL4, UAS:GCaMP6s* fish (6dpf). Pixels in panels D-F are coloured by their membership to *k*-means cluster centers. (G) *C*luster centers obtained from running *k*-means on data in D-F. (H-J) Heatmaps plotting temporal traces from segmented cells in dHbL (H; n = 5 fish), dHbM (I; n = 5 fish) and vHb (J; n = 8 fish). The cells are sorted into ON, OFF and Inhibitory categories that are separated by a horizontal black line. Mean traces of each category are plotted below the heatmaps. (K-L) Activity in axons of habenula neurons innervating the interpeduncular nucleus, in a *s1011tGAL4, UAS:GCaMP3* fish. Four different planes are shown, in lateral view. All domains show evoked activity, and responses appear to be organized according to region. Pixels are colour-coded according to the *k*-means clusters (L). In G-J and L, blue bars indicate the presence of light and vertical bold lines correspond to light onset while the dashed lines indicate light offset. a: anterior, p: posterior; l: lateral, m: medial. Scale bar = 25 µm.

Figure 4. Spatio-temporal characterization of light-evoked activity using high speed imaging. (A-F) Widefield imaging at 200 Hz. (A) Average of all frames in the time-lapse, to show morphology. This is a dorsal view of a 5 day old fish *elavl3:CaMP6f* fish. The habenula has been outlined in black. (B-F) Change in fluorescence relative to the preceding frame. An increase in fluorescence is seen in the thalamus (arrows) and in the left habenula (arrowhead). (G-I) Two photon imaging of the habenula in a *s1011tGAL4, UAS:GCaMP6s* fish, at 13 Hz. (G) Average of the time-lapse sequence, showing anatomy. The neuropil is indicated by the arrowhead. (H) Responses to pulses of light. Pixels are color-coded according to the traces in panel I. rHb: right habenula; lHb: left habenula. Panels A-E were smoothened using Gaussian blur with sigma = 1.7.

728 The time indicated is time since start of illumination with the excitation blue LED.

729 **Figure 5. The thalamus projection to the habenula.** (A) Dorsal view of the forebrain of
730 a *Et(SqKR11)* larva, in which habenula afferents from the entopeduncular nucleus are
731 labeled. The dorsal left neuropil (arrow) is weakly labeled. (B) Dorsal view of the
732 habenula of a *Et(SqKR11)* larva, following DiD injection into the dorsal neuropil of the left
733 habenula. The parapineal (arrow) has been retrogradely labeled. Habenula afferents
734 from the entopeduncular nucleus are labeled in red. (C) 80 µm deeper in the same fish,
735 showing label in the thalamus (white arrows). (D) Lateral view of another larva, in which
736 the dorsal left neuropil had been injected with DiD. The retrogradely labeled thalamic
737 neuropil is indicated (white arrow). The entopeduncular nucleus is indicated by the
738 yellow arrow. The inset shows a higher magnification labeled thalamic neuropil. Cell
739 bodies are labeled (white arrowhead). (E) A close up view of the neuropil retrogradely
740 labeled by DiD (cyan), in a fish where retinal ganglion cells had been labeled with DiI
741 (yellow). RGC terminals intermingle with fibers from DiD-labeled cells innervating the
742 neuropil (arrow). The arrowhead indicates a thalamic neuron labeled retrogradely with
743 DiD. (F, G) Dorsal view of the thalamus (F) and habenula (G) of a fish expressing Kaede
744 (red) under the control of the *GAL4s1020t* driver. Labelled cells are visible in the
745 thalamus (F, white arrowheads). Labelled neurites are visible in the thalamic neuropil (F,
746 yellow arrowheads) and in the habenula neuropils (G, arrowheads). GCaMP6f (green) is
747 broadly expressed in this fish. (H) Dorsal view of a 6-day-old fish, labeled with an anti-
748 vGlut1/2 antibody, which marks glutamatergic pre-synapses. All neuropils, including the
749 dorsal left (arrowhead), are labelled. (I) Dorsal view showing label with an anti-
750 GAD65/67 antibody. Labeled puncta are visible in the habenula neuropil (arrowhead).
751 No labeled cell bodies were detected in the habenula. (J) A *gad1b:RFP, vGlut2:GAL4,*
752 *UAS:eGFP* fish, with GABAergic cells indicated in magenta and glutamatergic cells

shown in green. Both cell types can be detected in the thalamus. The arrowhead indicates the neuropil of the putative nucleus rostrolateralis. (K) RFP expression in the thalamus of a *gad1b:RFP* fish. Arrowheads indicate neurites extending to the neuropil of the putative nucleus rostrolateralis. All panels except (A) and (H) are single optical sections. Pa: pallium; rHb: right habenula; lHb: left habenula; Th: thalamus. EN: entopeduncular nucleus; OT: optic tectum; *: auto-fluorescing pigment cell. Scale bar = 25 µm. Anterior is to the left in all cases.

Figure 6. Optogenetic stimulation of the thalamus triggers habenula activity. (A) Expression of ChR2-eYFP in the thalamus (arrowheads) of a 5 day old *s1020tGAL4, UAS:ChR2-eYFP, elavl3:GCaMP6f* fish. (B, C) Activity in the habenula of a ChR2-expressing fish, with (B) and without (C) blue LED stimulation of the thalamus. The images show the maximum projections of F/F_0 images for a 25-second period after blue LED illumination, following subtraction of maximum projections of the period before illumination (i.e. difference in activity before and after stimulation). (D-F) Heatmaps showing temporal activity from habenula neurons segmented in fish with (D, E) and without (F) ChR2. In D (n = 5 fish) and F (n = 2 fish), blue light pulse was given at the time indicated by the black dashed line. No blue light stimulation was given in E (n = 4 fish). Z-scores were calculated by subtracting each time traces by the total mean and dividing by the standard deviation. (G) Mean amplitude of z-scores before and after optogenetic stimulation. Each square stands for a stimulus trial. Amplitude difference before and after stimulation in ChR2-expressing fish: mean ± 95% CI: 1 Hz: 0.43 ± 0.56, 2 Hz: 0.72 ± 0.35, 4 Hz: 0.89 ± 0.28 and 8 Hz : 1.05 ± 0.18; in siblings: 0.21 ± 0.51. Scale bar = 25 µm.

Figure 7. Light-evoked activity in the thalamus. (A-E) Evoked activity in five different focal planes, from dorsal to ventral, of a 5-day-old fish expressing GCaMP6s in thalamic

778 neurons. Responses are seen in cell bodies (arrows) and in the thalamic neuropil
779 (arrowheads). The colours represent k-means cluster center (F). (G-J) Lateral view of
780 light-evoked activity in the thalamus. (G) The region imaged. (H) Average projection of a
781 lateral view of an *elavl3:GCaMP6f* fish, showing the thalamic neuropil (arrowhead).
782 (I) The response in this fish to four pulses of blue light. Pixels are colored according to
783 the *k*-means cluster center (J). (K-P) The effect of eye removal on light-evoked activity in
784 the thalamus. (K-M) Response in a control (K-M) and eye lesioned fish (N-P), color-
785 coded according to the k-means cluster centers in (L) and (O) respectively. (M, P)
786 Trajectory of the thalamic response using the first two principal components (PC1 and
787 PC2) in control (M) and lesioned (P) fish, colored according to the wedges in panels L
788 and O to indicate the direction of the trajectories in Principal Component space following
789 light ON and OFF. Controls, but not lesioned fish, show a reproducible response to light.
790 Insets in M and P show the correlation coefficient (CC) of the first 20 PCs with a trace
791 mimicking light evoked activity (see Methods). Unlike controls, the top 20 PCs in the eye
792 lesioned fish showed weak correlation and did not pick up any light evoked response.
793 (Q) Correlation coefficients between response of each thalamic pixel and a trace
794 mimicking response to blue light in multiple *s1020tGAL4, UAS:GCamp6s* fish. All
795 positive correlation coefficients are plotted here. Each boxplot represents one fish. The
796 black diamonds are outliers (see Methods). (R-S) Heatmaps showing the number of
797 pixels with correlation coefficient > 0.5 in control (R) and fish lacking eyes (S). Traces
798 below show the mean of all the pixels (black traces) and standard error of mean (shaded
799 region). In panels F, J, L, O and R-S, light onset is indicated by the solid line, while light
800 offset is indicated by the dashed line. Presence of light is indicated by the blue bars. a:
801 anterior; p: posterior; d:dorsal, v: ventral. Th: thalamus; Hb:habenula. PC: Principal
802 component, PC1: First principal component, PC2: Second principal component, CC:
803 Correlation Coefficient. Scale bar = 25 µm. The drawing in panel G was obtained from

804 www.uoneuro.uoregon.edu

805

806 **Figure 8. Asymmetric light-evoked activity in thalamic axon terminals in the dorsal**
807 **habenula.** (A) Standard deviation projection of a time-series recording of the dorsal
808 habenula of a 6-day-old *s1020tGAL4,UAS:GCaMP6s* fish. The bright pixels are those
809 with large change in activity. The surrounding skin, which was auto-fluorescent, has
810 been masked. The dorsal left neuropil is indicated with a yellow arrowhead while the
811 dorsal right neuropil is indicated with a green arrowhead. Habenula neurons are dimly
812 auto-fluorescent. (B) Pixels within the dorsal neuropils with activity above 1 standard
813 deviation, colour-coded yellow for left habenula and green for right habenula. This
814 criteria included all terminals in the neuropils. (C) Pixels colour-coded according to
815 whether they responded to light ON (cyan) or OFF (magenta). A relatively large
816 proportion of pixels in the left neuropil responded, compared to the right (compare C with
817 B). Pixels were selected by correlating their activity to a square wave form that was 1
818 during light ON (for ON pixels) and 1 during light OFF (for OFF pixels). Pixels with
819 correlation coefficient greater than 0.5 were selected. (D-I) Analysis of multiple fish
820 (n=7). (D) Boxplot of total number of pixels present in the left and right habenula. The
821 number of terminals in left and right habenula were comparable across fish. (E) Number
822 of terminals responding to light ON or light OFF. In D and E, each circle represent data
823 from a single fish. p-value was obtained using non parametric paired Wilcoxon signed
824 rank test. W is sum of the ranks, Z is the test statistic, and r is the effect size. (F-G) Heat
825 maps of activity from all fish, in all thresholded pixels in the left habenula (F), the right
826 habenula (G), and in pixels corresponding to light ON (H) and light OFF (I). Each line
827 corresponds to a single pixel. Panels below show the average of the heat maps above.
828 The shaded region is standard error of mean. Blue boxes indicate when light was
829 delivered. Light onset is indicated by the solid line, while light offset is indicated by the

dashed line. Anterior is to the top in panels A-C. Scale bar = 25 µm.

Figure 9. The effect of lesioning the thalamus on habenula response to light. (A-C) Dorsal view of an 8-day-old *elavl3:GCaMP6f* fish, showing neural responses before (A) and after (C) lesioning the region of the thalamic neuropil that responds to light (yellow arrowheads in panel A). Pixels in panels A and C are colored according to their activity, as indicated by traces in panel B. The prominent sustained response to light (cyan pixels) is reduced after lesion. (D) The extent of lesion, shown in magenta. (E-G) Habenula activity before (E) and after (G) lesion of the thalamic neuropil. Pixels are colored according to the traces in (F). There is a reduction in the sustained response to light, but some activity that is not stimulus-locked can be seen. (H) The habenula after lesion of AF9, with pixels colored according to the traces in panel (I). (J-M) Heatmaps showing activity in segmented cells before (J) and after (K) AF9 lesion, and before (L) and after (M) thalamic neuropil lesion in one fish. Panels below show mean (black trace) and standard error of mean (shaded region). Light evoked activity is missing following this lesion. (N) Boxplot showing number of cells in one plane of the dorsal left habenula that are excited by blue light, following lesion of the thalamic neuropil (n = 12 fish), or AF7 (n = 2 fish) or AF9 (n = 3 fish), or before lesion (n = 5 fish). P-value was obtained using non parametric Wilcoxon rank sum test. Z is the test statistic, and r is the effect size. The statistical comparisons were made between before lesion and after lesion. a: anterior; p: posterior; Pa: pallium; rHb: right habenula. Images are all single optical sections. Scale bar = 25 µm.

Figure 10. A potential projection from the ventral lateral geniculate nucleus to the habenula in mouse. Anterograde label was performed by injecting recombinant adeno associated virus into the ventral lateral geniculate nucleus (Oh et al., 2014). 0.33 mm^3

was injected into Bregma (-2.46, 2.6, 2.36, 0) of a p56 slc32a1-IRES-Cre mouse, which expresses Cre in GABAergic neurons. (A) Coronal view, showing an overview of the label. (B) A high magnification of the area boxed in panel A, showing labeled fibers in the habenula. mHb: medial habenula. These images are from http://connectivity.brain-map.org/projection/experiment/siv/267538006?imageId=267538231&imageType=TWO_PHOTON,SEGMENTATION&initImage=TWO_PHOTON&x=14704&y=7847&z=3.

Movie 1. Habenula neurons do not project to the thalamus. 3D rendition of habenula projection in a zebrafish larva, visualized by expression of RFP under the *narp* promoter (red) and eGFP under the *brn3a* promoter (green). There is a clear projection to the interpeduncular nucleus (IPN), but not to the thalamus.

Movie2. Thalamic neurons project to the habenula. Z-stack of a *s1020t:GAL4, UAS: Kaede, elavl3:GCaMP6f* fish. Thalamic neurons are shown in red, and they can be seen to project to the neuropils of the habenula. Red label also appears in streaks in the lateral habenula. Anterior is to the top.

Movie 3. GAD65/67 label in a zebrafish larva. z-stack of a s*1011t:GAL4, UAS:GCaMP3* transgenic fish, after immuno-labelling with an antibody to GAD65/67 (magenta). The stack goes from dorsal to ventral. GAD65/67 label is visible in neuropils of the habenula; puncta can be seen between cells in the lateral regions of the habenula in more ventral planes. GAD65/67 labeled cells are visible in the deep focal planes, but these do not express GCaMP3. The location of GAD65/67 expressing cells correlates with the thalamus. S1011Et drives GAL4 expression in the habenula, medial pallium and anterior-lateral pallium. This is a dorsal view, with anterior to the left.

Movie 4. Z-stack of 6 day old *gad1b:RFP, elavl3:GCaMP6f* fish. GABAergic neurons (magenta) are visible in the thalamus, below the habenula. Anterior is to the left. The

880 stack goes from dorsal to ventral.

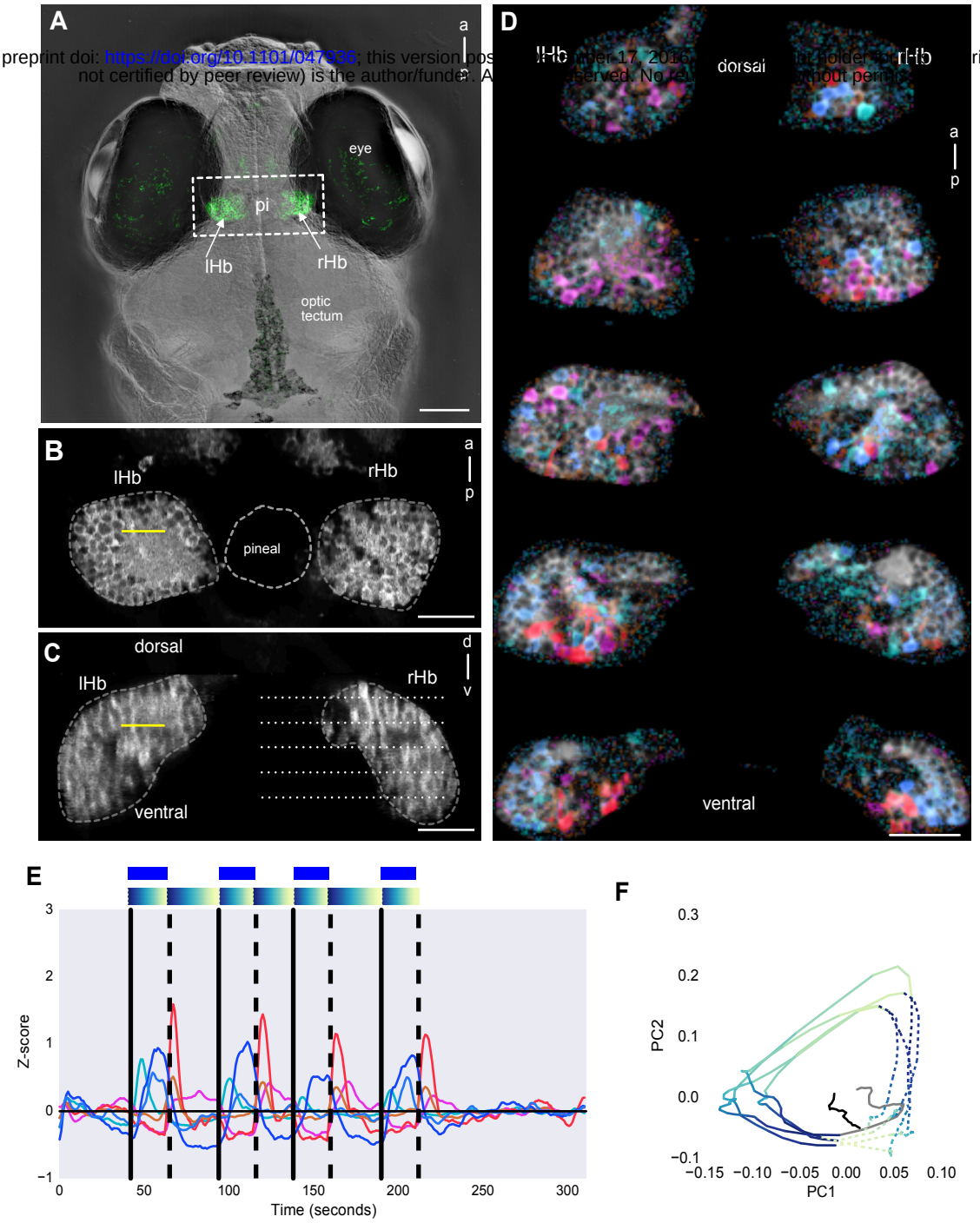

Figure 1. The larval zebrafish habenula has a broad and complex response to change in irradiance. (A) Dorsal view of the head of a live 7 day-old fish, with GCaMP3 expression in the habenula (arrows) under the control of the s1011t GAL4 driver. (B) A single two-photon slice through the dorsal habenula of the fish in panel A (boxed region). (C) A yz reconstruction at the point indicated by the yellow line in panel B, showing a transverse view of the habenula. The dotted lines indicate imaging planes separated by 10 µm. The yellow line indicates the plane imaged in B. Dashed lines show the border of the habenula. (D) Spatial distribution of responses in the habenula of one fish (7 dpf) to pulses of light. 5 planes are shown here. The colors are coded according to the temporal pattern of response, as indicated in (E). Images were collected at a rate of 1 stack/second, and four pulses of light were delivered for 20 seconds each, with variable inter-stimulus interval. (E) Centers of k-means clusters corresponding to colors of pixels in (D). Cluster centers in (D) and the corresponding pixels in (E) indicating responses to light ON are colored in shades of blue and light OFF in shades of red. The horizontal black line represents Z-score of 0. (F) Trajectory of the habenula response in two-dimensional state space, using the first two principal components (PC1 and PC2). Traces are color-coded according to the wedges in panel E, to represent direction in which change in irradiance drives the neural state. In panels E and F, the bold lines correspond to light onset while the dashed lines indicate offset. The presence of light is also indicated by the blue bars. lHb: left habenula; rHb: right habenula. a: anterior; p: posterior. d: dorsal; v: ventral Scale bar = 100 µm in panel A, 25 µm elsewhere.

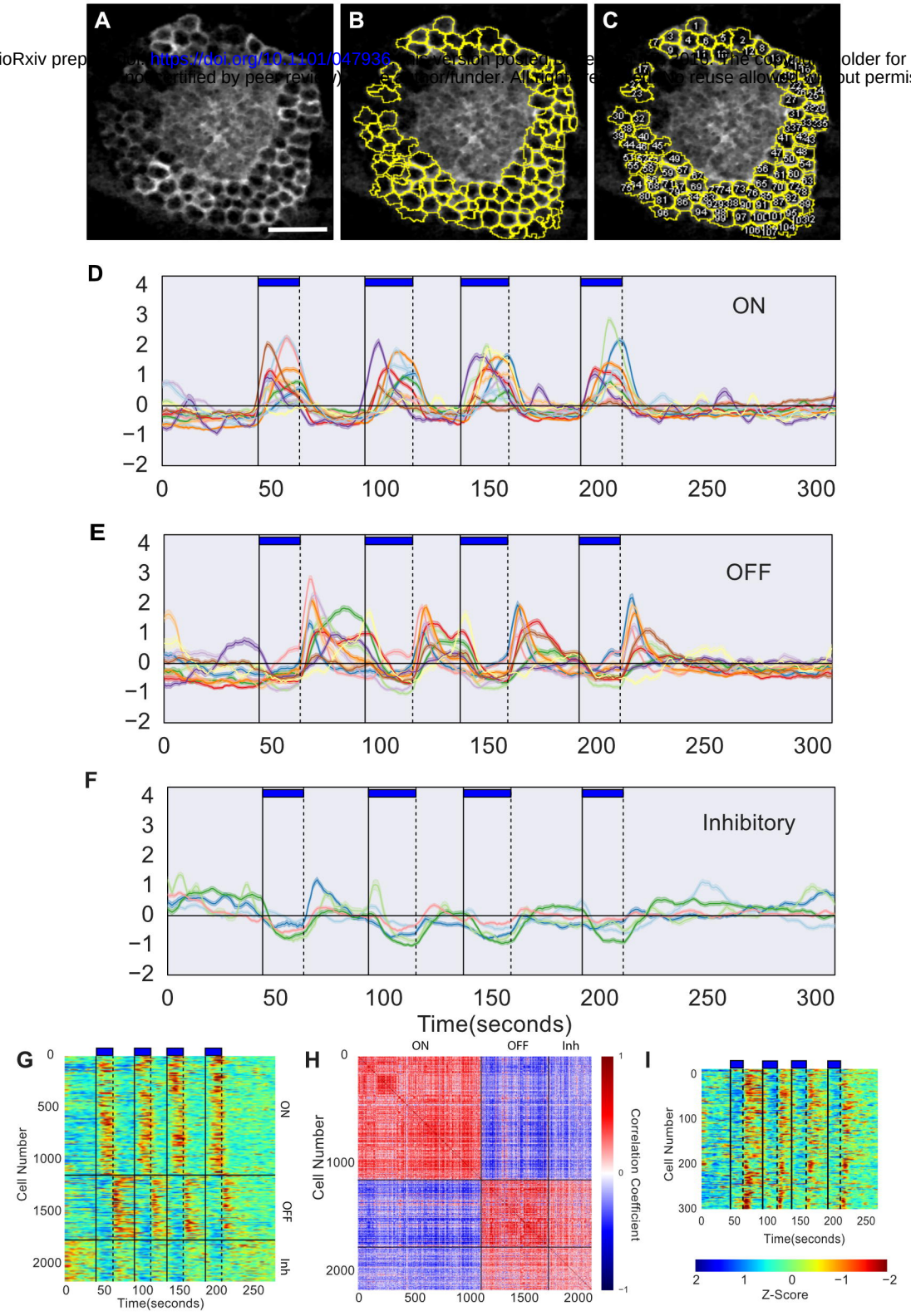

Figure 2. Habenula response to irradiance change is reproducible. (A-C) Segmentation of habenula neurons using a semi-automated algorithm (see Methods). (D-F) K-means cluster analysis of segmented habenula neuron responses to pulses of blue light in 6 fish (7-8 dpf). Traces show cluster centroids, with shaded regions indicating standard error of the mean. Clusters were grouped by their temporal activity pattern and clusters with excitation to light ON (D) or OFF (E), or inhibition to light (Inhibitory, F) were seen. Clusters without evoked responses are not shown. (G) Activity traces of each cell from the 6 fish grouped into ON, OFF and Inhibitory (Inh) categories based on their membership to the clusters shown in D-F. Horizontal black lines divide the categories. (H) Correlation between activity of cells belonging to ON, OFF and Inhibitory (Inh) clusters shown in D-F. In general, the ON and OFF responding cells were uncorrelated (correlation coefficient < 0). Vertical and horizontal black lines divide ON, OFF and Inhibitory categories. (I) Activity traces of cells in ON and OFF clusters that showed high correlation with the other category (313 of 1767 cells). The traces showed that this correlation may be due to OFF cells showing slow decay in fluorescence following light ON. Manual inspection of the traces did not reveal any cells that responded reliably to both light ON and OFF. Colorbar for panels G and I is shown below panel I. Scale bar = 25 µm.

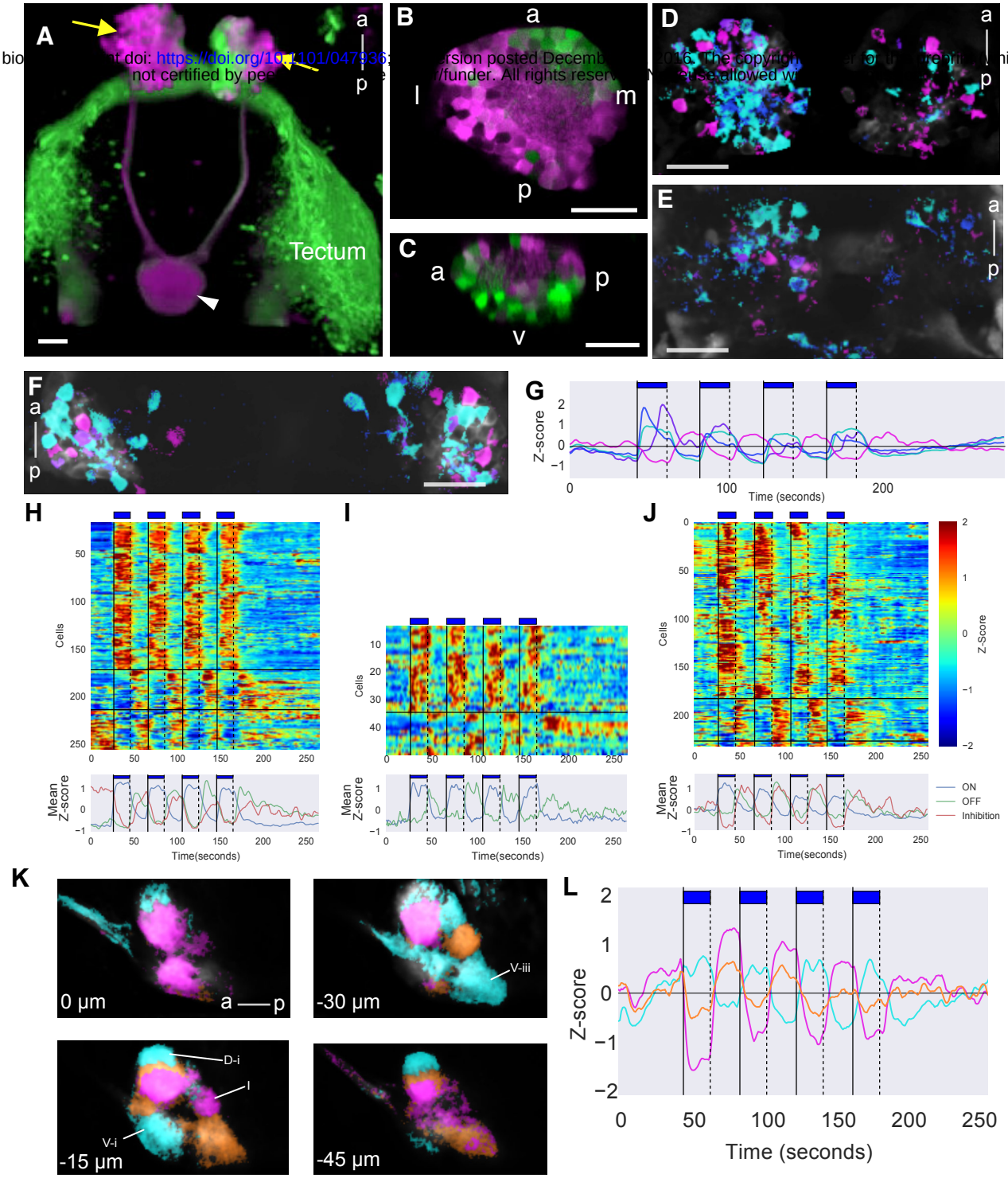

Figure 3. The response of different habenula subdomains to change in irradiance. (A-C) A *narp:GAL4, UAS:DsRed, Brn3a:eGFP* larva, with label in the dorsal habenula (arrows) and projection to the IPN (arrowhead). A coronal (B) and reconstructed sagittal (C) section through the left habenula, with dHbM in green and dHbL in magenta. (D) Spatial distribution of responses in the dorsal habenula of a *narp:GAL4, UAS:GCaMP6s* fish (8dpf). (E). Responses of non-DsRed cells in the dorsal habenula of a *elavl3:GCaMP6f, narp:GAL4, UAS:DsRed* fish (6dpf). (F) Responses in the ventral habenula of a *dao:GAL4, UAS:GCaMP6*s fish (6dpf). Pixels in panels D-F are coloured by their membership to k-means cluster centers. (G) Cluster centers obtained from running k-means on data in D-F. (H-J) Heatmaps plotting temporal traces from segmented cells in dHbL (H; n = 5 fish), dHbM (I; n = 5 fish) and vHb (J; n = 8 fish). The cells are sorted into ON, OFF and Inhibitory categories that are separated by a horizontal black line. Mean traces of each category are plotted below the heatmaps. (K-L) Activity in axons of habenula neurons innervating the interpeduncular nucleus, in a *s1011tGAL4, UAS:GCaMP3* fish. Four different planes are shown, in lateral view. All domains show evoked activity, and responses appear to be organized according to region of the IPN. Pixels are colour-coded according to the k-means clusters (L). In G-J and L, blue bars indicate the presence of light and vertical bold lines correspond to light onset while the dashed lines indicate light offset. a: anterior, p: posterior; l: lateral, m: medial. Scale bar = 25 µm.

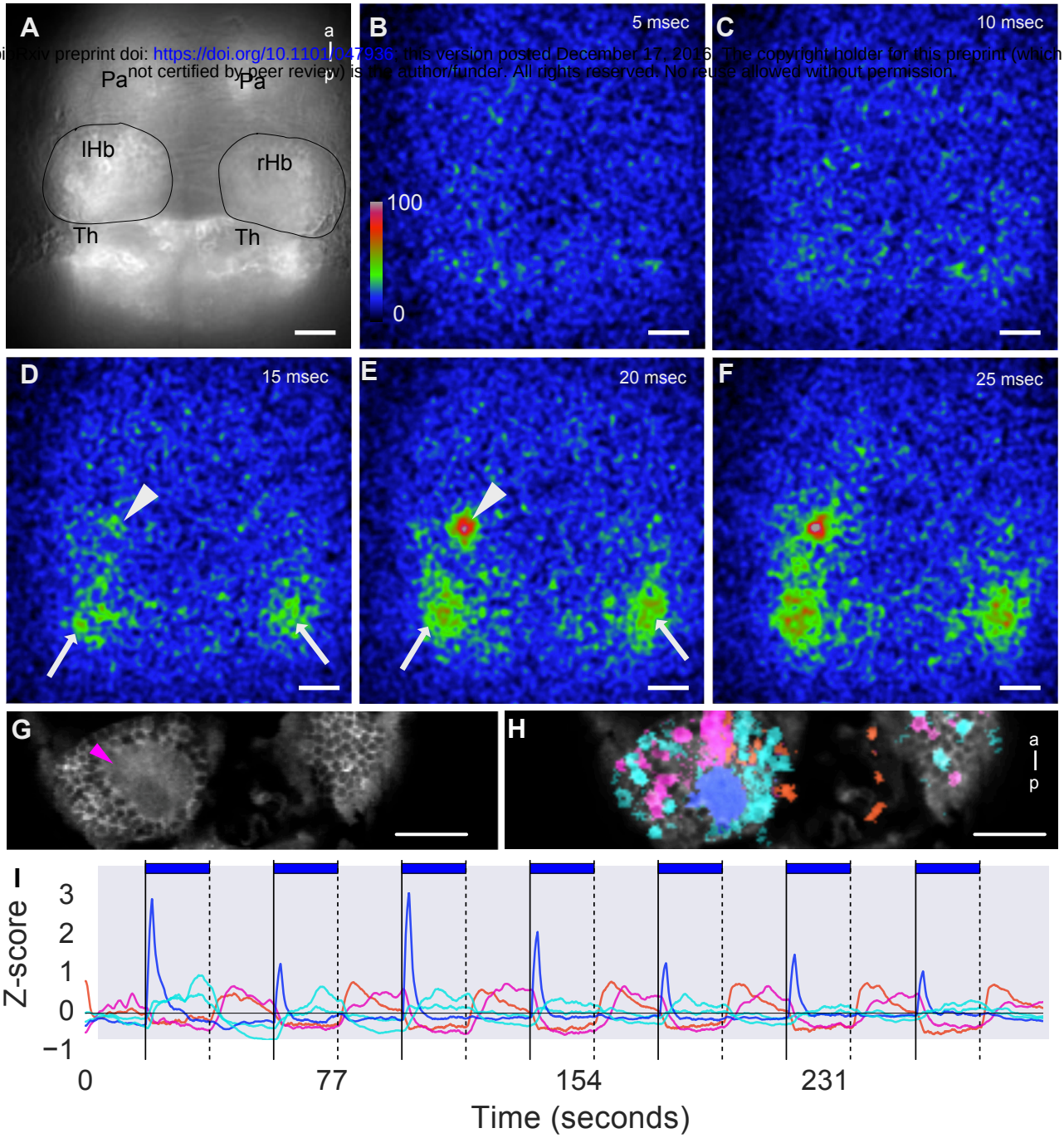

Figure 4. Spatio-temporal characterization of light-evoked activity using high speed imaging. (A-F) Widefield imaging at 200 Hz. (A) Average of all frames in the time-lapse, to show morphology. This is a dorsal view of a 5 day old fish *elavl3:CaMP6f* fish. The habenula has been outlined in black. (B-F) Change in fluorescence relative to the preceding frame. An increase in fluorescence is seen in the thalamus (arrows) and in the left habenula (arrowhead). (G-I) Two photon imaging of the habenula in a *s1011tGAL4, UAS:GCaMP6s* fish, at 13 Hz. (G) Average of the time-lapse sequence, showing anatomy. The neuropil is indicated by the arrowhead. (H) Responses to pulses of light. Pixels are color-coded according to the traces in panel I. rHb: right habenula; lHb: left habenula. Panels A-E were smoothened using Gaussian blur with sigma = 1.7. The time indicated is time since start of illumination with the excitation blue LED.

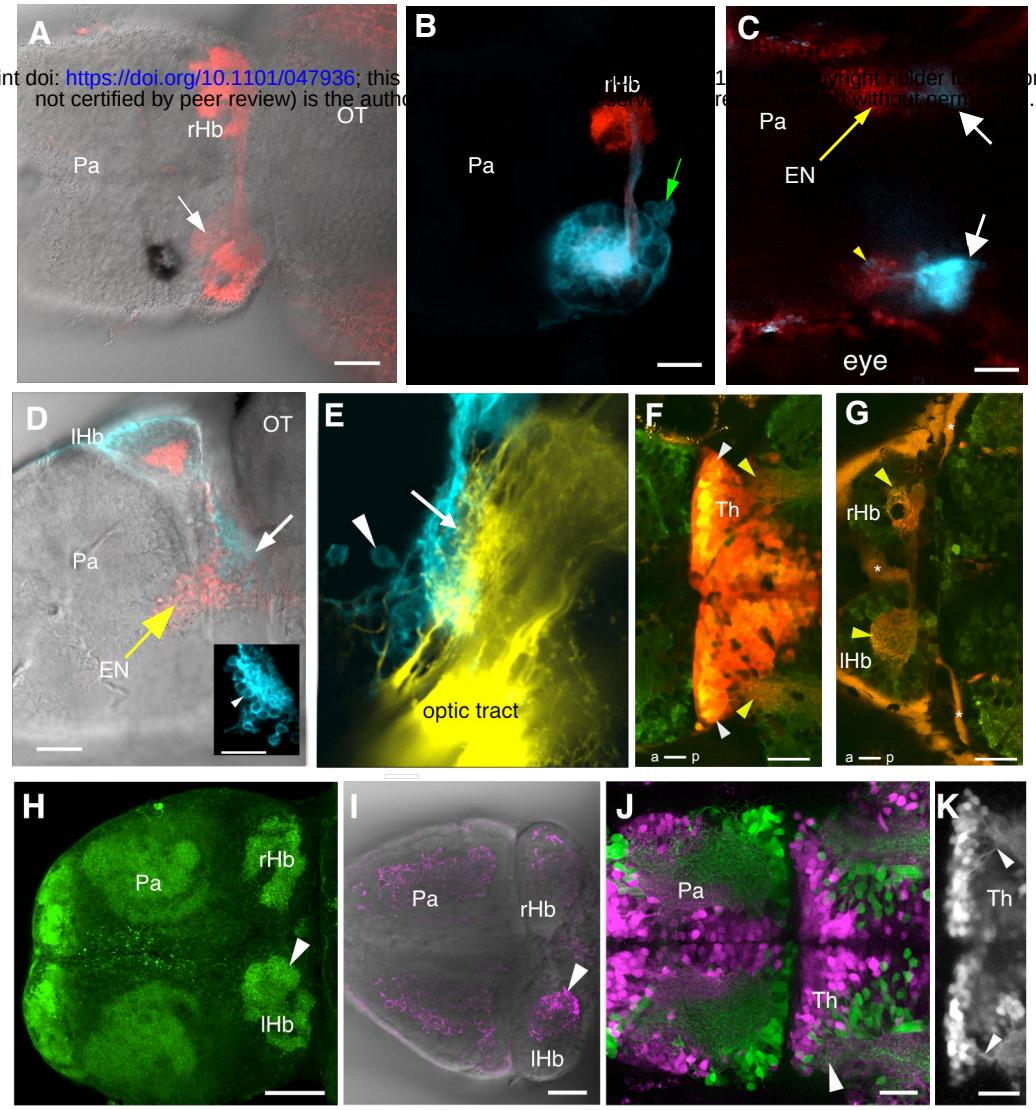

Figure 5. The thalamus projection to the habenula. (A) Dorsal view of the forebrain of a *Et(SqKR11)* larva, in which habenula afferents from the entopeduncular nucleus are labeled. The dorsal left neuropil (arrow) is weakly labeled. (B) Dorsal view of the habenula of a *Et(SqKR11)* larva, following DiD injection into the dorsal neuropil of the left habenula. The parapineal (arrow) has been retrogradely labeled. Habenula afferents from the entopeduncular nucleus are labeled in red. (C) 80 µm deeper in the same fish, showing label in the thalamus (white arrows). One retrogradely cell in the entopeduncular nucleus is visible (yellow arrowhead). (D) Lateral view of another larva, in which the dorsal left neuropil had been injected with DiD. The retrogradely labeled thalamic neuropil is indicated (white arrow). The entopeduncular nucleus is indicated by the yellow arrow. The inset shows a higher magnification labeled thalamic neuropil. Cell bodies are labeled (white arrowhead). (E) A close up view of the neuropil retrogradely labeled by DiD (cyan), in a fish where retinal ganglion cells had been labeled with DiI (yellow). RGC terminals intermingle with fibers from DiD-labeled cells innervating the neuropil (arrow). The arrowhead indicates a thalamic neuron labeled retrogradely with DiD. (F, G) Dorsal view of the thalamus (F) and habenula (G) of a fish expressing Kaede (red) under the control of the *s1020tGAL4* driver. Labelled cells are visible in the thalamus (F, white arrowheads). Labelled neurites are visible in the thalamic neuropil (F, yellow arrowheads) and in the habenula neuropils (G, arrowheads). GCaMP6f (green) is broadly expressed in this fish. (H) Dorsal view of a 6-day-old fish, labeled with an anti-vGlut1/2 antibody, which marks glutamatergic pre-synapses. All neuropils, including the dorsal left (arrowhead), are labelled. (I) Dorsal view showing label with an anti-GAD65/67 antibody. Labeled puncta are visible in the habenula neuropil (arrowhead). No labeled cell bodies were detected in the habenula. (J) A *gad1b:RFP, vGlut2:GAL4, UAS:eGFP* fish, with GABAergic cells indicated in magenta and glutamatergic cells shown in green. Both cell types can be detected in the thalamus. The arrowhead indicates the neuropil of the putative nucleus rostrolateralis. (K) RFP expression in the thalamus of a *gad1b:RFP* fish. Arrowheads indicate neurites extending to the neuropil of the putative nucleus rostrolateralis. All panels except (A) and (H) are single optical sections. Pa: pallium; rHb: right habenula; lHb: left habenula; Th: thalamus. EN: entopeduncular nucleus; OT: optic tectum; *: auto-fluorescing pigment cell. Scale bar = 25 µm. Anterior is to the left in all cases.

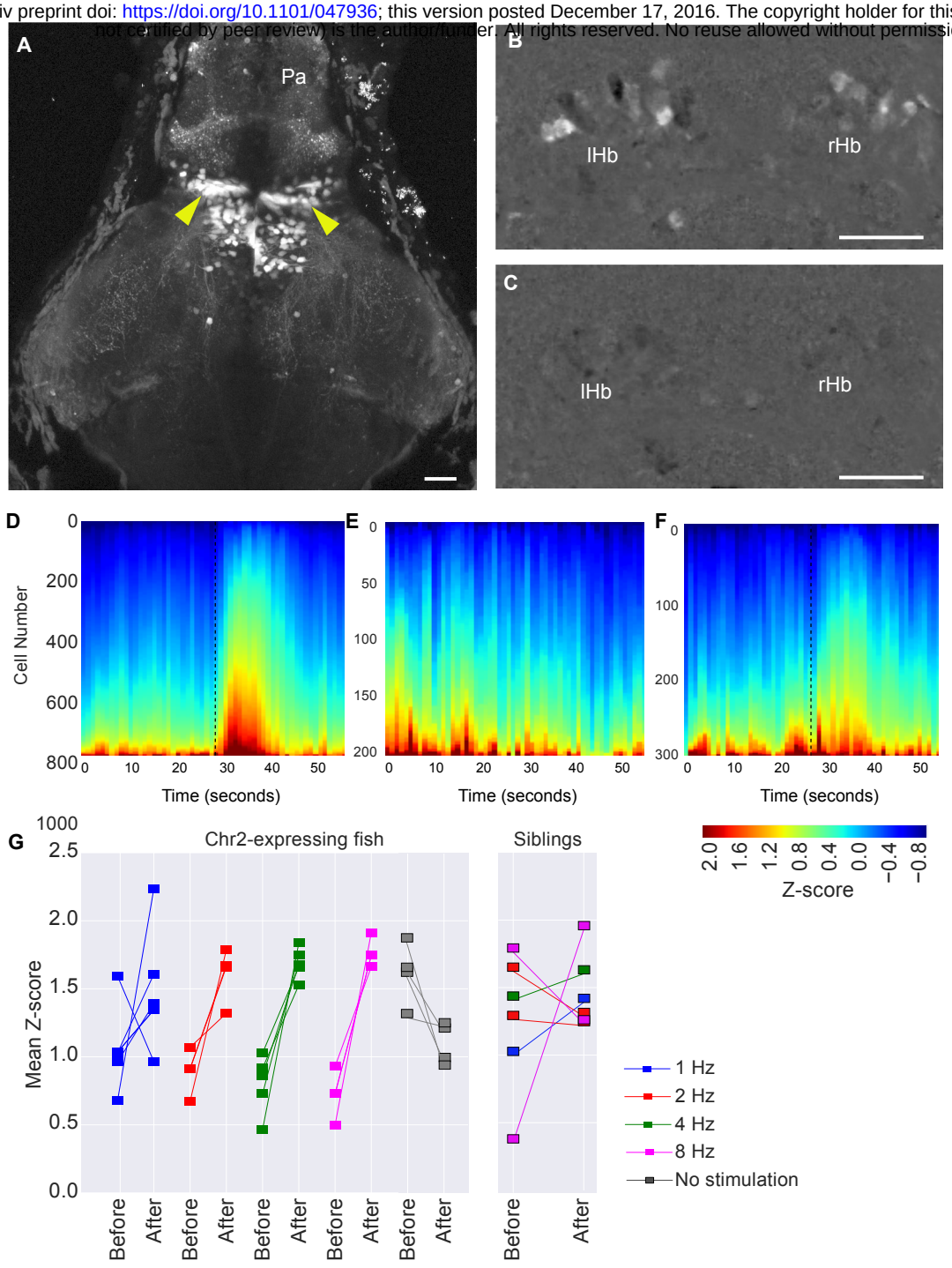

Figure 6. Optogenetic stimulation of the thalamus triggers habenula activity. (A) Expression of ChR2-eYFP in the thalamus (arrowheads) of a 5 day old *s1020t:GAL4, UAS:ChR2-eYFP, elavl3:GCaMP6f* fish. (B, C) Activity in the habenula of a ChR2-expressing fish, with (B) and without (C) blue LED stimulation of the thalamus. The images show the maximum projections of F/F_0 images for a 25-second period after blue LED illumination, following subtraction of maximum projections of the period before illumination (i.e. difference in activity before and after stimulation). (D-F) Heatmaps showing temporal activity from cells segmented in fish with (D, E) and without (F) ChR2. In D (n = 5 fish) and F (n = 2 fish), blue light pulse was given at the time indicated by the black dashed line. No blue light stimulation was given in E (n = 4 fish). Z-scores were calculated by subtracting each time traces by the total mean and dividing by the standard deviation. (G) Mean amplitude of z-scores before and after optogenetic stimulation. Each square stands for a stimulus trial. Amplitude difference before and after stimulation in ChR2-expressing fish: mean ± 95% CI: 1 Hz: 0.43 ± 0.56, 2 Hz: 0.72 ± 0.35, 4 Hz: 0.89 ± 0.28 and 8 Hz : 1.05 ± 0.18; in siblings: 0.21 ± 0.51. Scale bar = 25 µm.

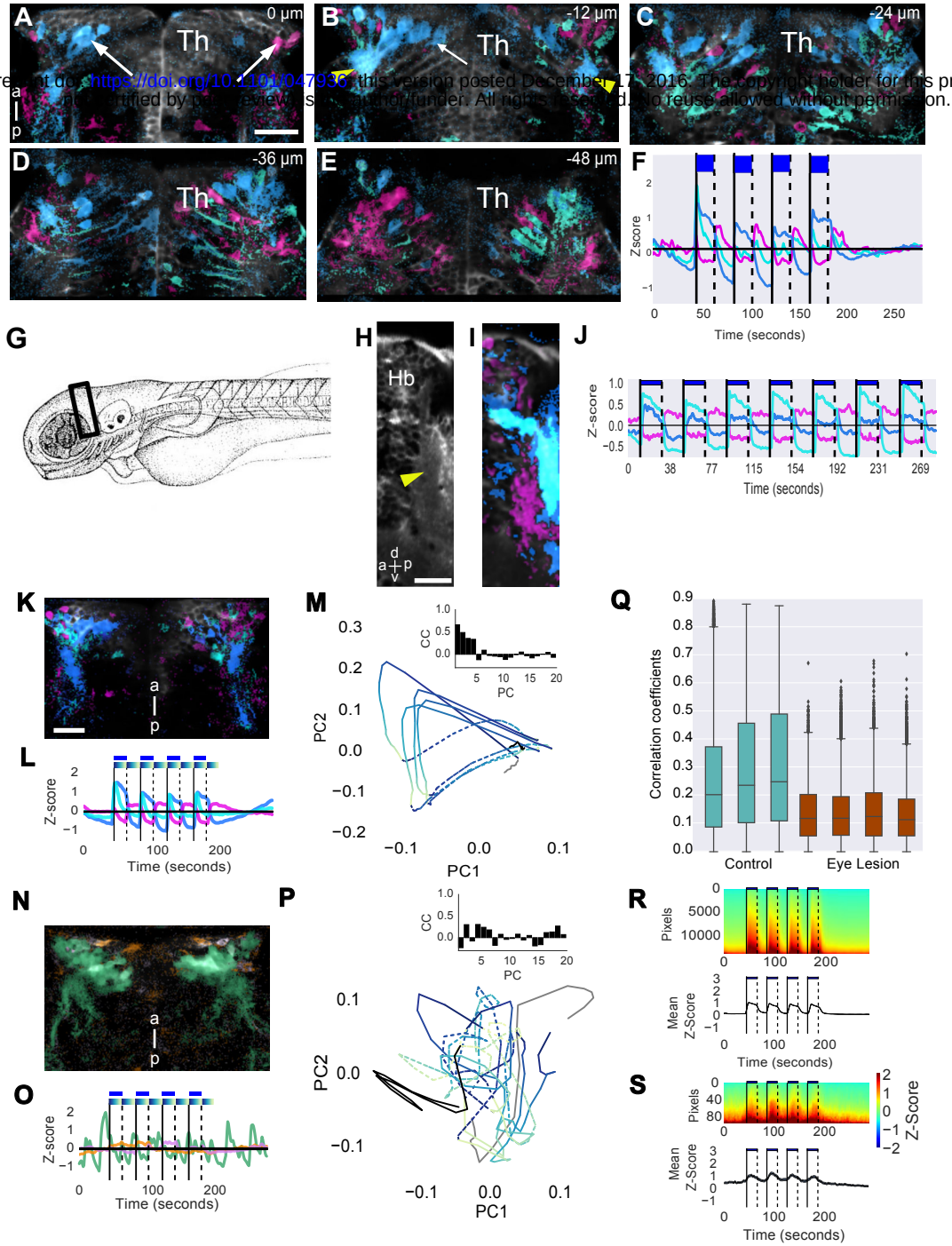

Figure 7. Light-evoked activity in the thalamus. (A-E) Evoked activity in five different focal planes, from dorsal to ventral, of a 5-day-old fish expressing GCaMP6s in thalamic neurons under the s1020t driver. Responses are seen in cell bodies (arrows) and in the thalamic neuropil (arrowheads). The colours represent k-means cluster centers (F). (G-J) Lateral view of light-evoked activity in the thalamus. (G) The region imaged. (H) Average projection of a lateral view of an *elavl3:GCaMP6f* fish, showing the thalamic neuropil (arrowhead). (I) The response in this fish to four pulses of blue light. Pixels are colored according to the k-means cluster centers (J). (K-P) The effect of eye removal on light-evoked activity in the thalamus. (K-M) Response in a control (K-M) and eye lesioned fish (N-P), color-coded according to the k-means cluster centers in (L) and (O) respectively. (M, P) Trajectory of the thalamic response using the first two principal components (PC1 and PC2) in control (M) and lesioned (P) fish, colored according to the wedges in panels L and O to indicate the direction of the trajectories in Principal Component space following light ON and OFF. Controls, but not lesioned fish, show a reproducible response to light. Insets in M and P show the correlation coefficient (CC) of the first 20 PCs with a trace mimicking light evoked activity (see Methods). Unlike controls, the top 20 PCs in the eye lesioned fish showed weak correlation and did not pick up any light evoked response. (Q) Correlation coefficients between response of each thalamic pixel and a trace mimicking response to blue light in multiple *s1020tGAL4, UAS:GCamp6s* fish. All positive correlation coefficients are plotted here. Each boxplot represents one fish. The black diamonds are outliers (see Methods). (R-S) Heatmaps showing the number of pixels with correlation coefficient > 0.5 in control (R) and fish lacking eyes (S). Traces below show the mean of all the pixels (black traces) and standard error of mean (shaded region). In panels F, J, L, O and R-S, light onset is indicated by the solid line, while light offset is indicated by the dashed line. Presence of light is indicated by the blue bars. a: anterior; p: posterior; d:dorsal, v: ventral. Th: thalamus; Hb:habenula. PC: Principal component, PC1: First principal component, PC2: Second principal component, CC: Correlation Coefficient. Scale bar = 25 µm. The drawing in panel G was obtained from www.uoneuro.uoregon.edu

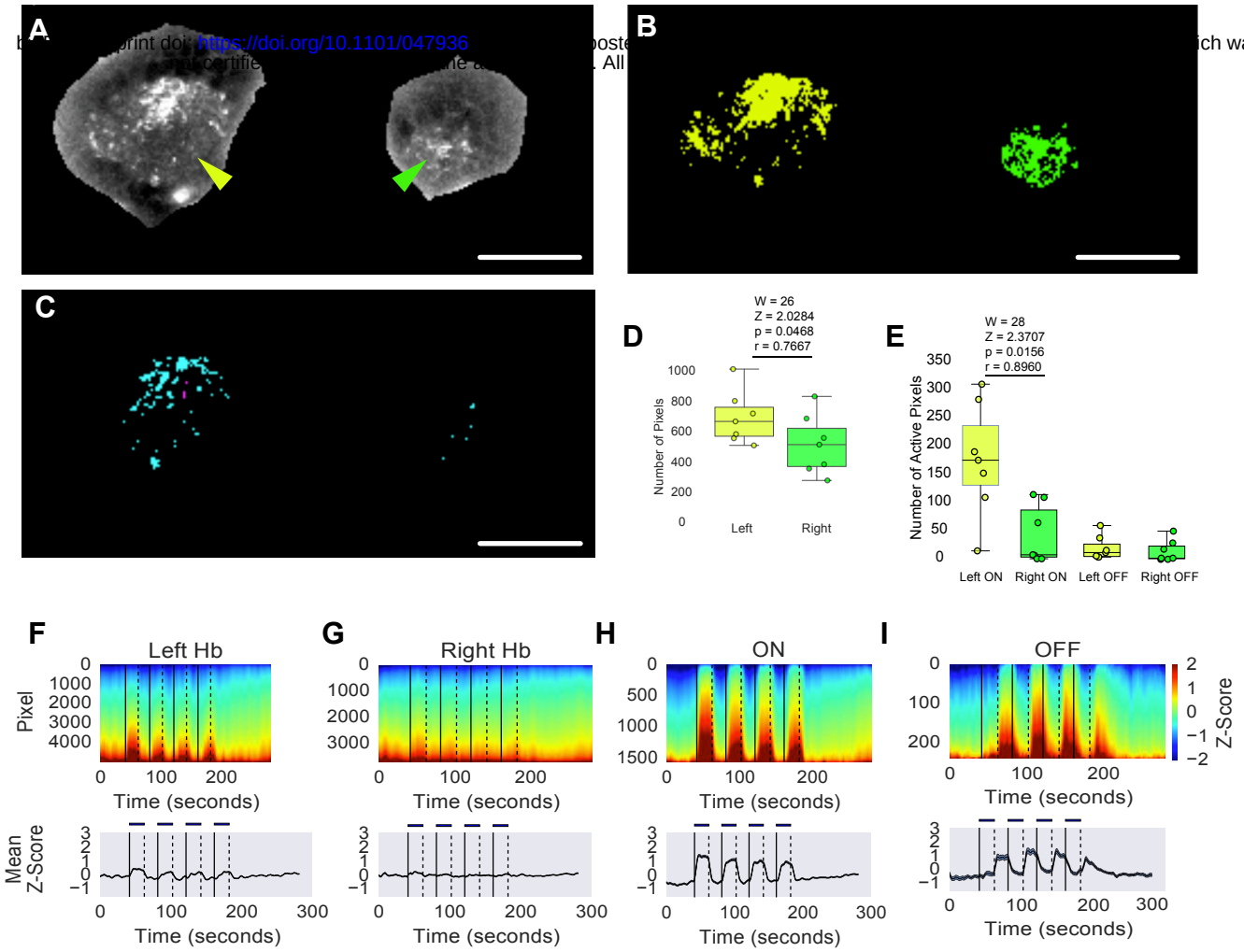

Figure 8. Asymmetric light-evoked activity in thalamic axon terminals in the dorsal habenula. (A) Standard deviation projection of a time-series recording of the dorsal habenula of a 6-day-old *s1020tGAL4,UAS:GCaMP6s* fish. The bright pixels are those with large change in activity. The surrounding skin, which was auto-fluorescent, has been masked. The dorsal left neuropil is indicated with a yellow arrowhead while the dorsal right neuropil is indicated with a green arrowhead. Habenula neurons are dimly auto-fluorescent. (B) Pixels within the dorsal neuropils with activity above 1 standard deviation, colour-coded yellow for left habenula and green for right habenula. This criteria included all terminals in the neuropils. (C) Pixels colour-coded according to whether they responded to light ON (cyan) or OFF (magenta). A relatively large proportion of pixels in the left neuropil responded, compared to the right (compare C with B). Pixels were selected by correlating their activity to a square wave form that was 1 during light ON (for ON pixels) and 1 during light OFF (for OFF pixels). Pixels with correlation coefficient greater than 0.5 were selected. (D-I) Analysis of multiple fish (n=7). (D) Boxplot of total number of pixels present in the left and right habenula. The number of terminals in left and right habenula were comparable across fish. (E) Number of terminals responding to light ON or light OFF. In D and E, each circle represent data from a single fish. p-value was obtained using non parametric paired Wilcoxon signed rank test. W is sum of the ranks, Z is the test statistic, and r is the effect size. (F-G) Heat maps of activity from all fish, in all thresholded pixels in the left habenula (F), the right habenula (G), and in pixels corresponding to light ON (H) and light OFF (I). Each line corresponds to a single pixel. Panels below show the average of the heat maps above. The shaded region is standard error of mean. Blue boxes indicate when light was delivered. Light onset is indicated by the solid line, while light offset is indicated by the dashed line. Anterior is to the top in panels A-C. Scale bar = 25 µm.

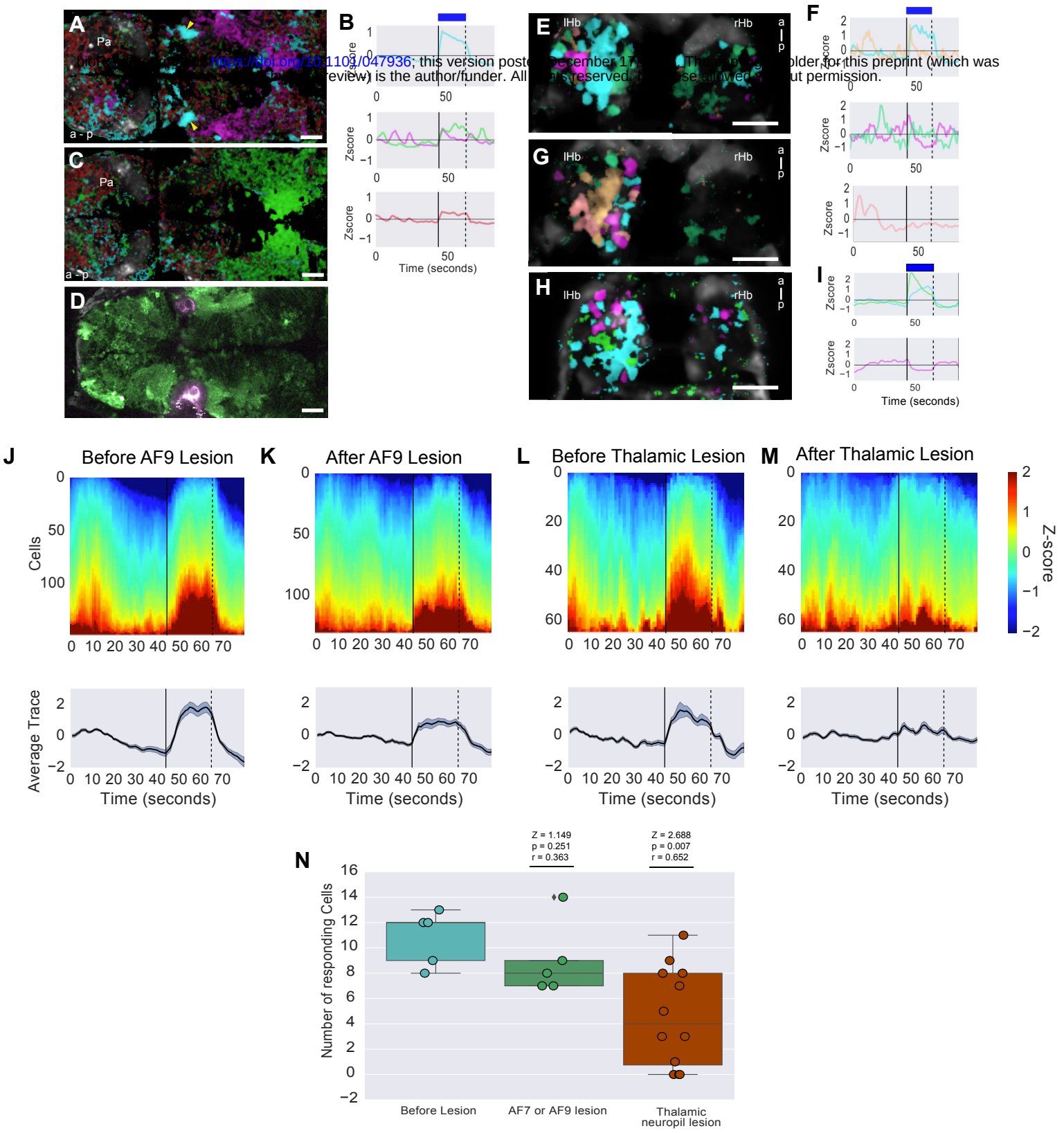

Figure 9. The effect of lesioning the thalamus on habenula response to light. (A-C) Dorsal view of an 8-day-old elavl3:GCaMP6f fish, showing neural responses before (A) and after (C) lesioning the region of the thalamic neuropil that responds to light (yellow arrowheads in panel A). Pixels in panels A and C are colored according to their activity, as indicated by traces in panel B. The prominent sustained response to light (cyan pixels) is reduced after lesion. (D) The extent of lesion, shown in magenta. (E-G) Habenula activity before (E) and after (G) lesion of the thalamic neuropil. Pixels are colored according to the traces in (F). There is a reduction in the sustained response to light, but some activity that is not stimulus-locked can be seen. (H) The habenula after lesion of AF9, with pixels colored according to the traces in panel (I). (J-M) Heatmaps showing activity in segmented cells before (J) and after (K) AF9 lesion, and before (L) and after (M) thalamic neuropil lesion in one fish. Panels below show mean (black trace) and standard error of mean (shaded region). Light evoked activity is missing following this lesion. (N) Boxplot showing number of cells in one plane of the dorsal left habenula that are excited by blue light, following lesion of the thalamic neuropil (n = 12 fish), or AF7 (n = 2 fish) or AF9 (n = 3 fish), or before lesion (n = 5 fish). P-value was obtained using non parametric Wilcoxon rank sum test. Z is the test statistic, and r is the effect size. The statistical comparisons were made between before lesion and after lesion. a: anterior; p: posterior; Pa: pallium; rHb: right habenula. Images are all single optical sections. Scale bar = 25 µm.

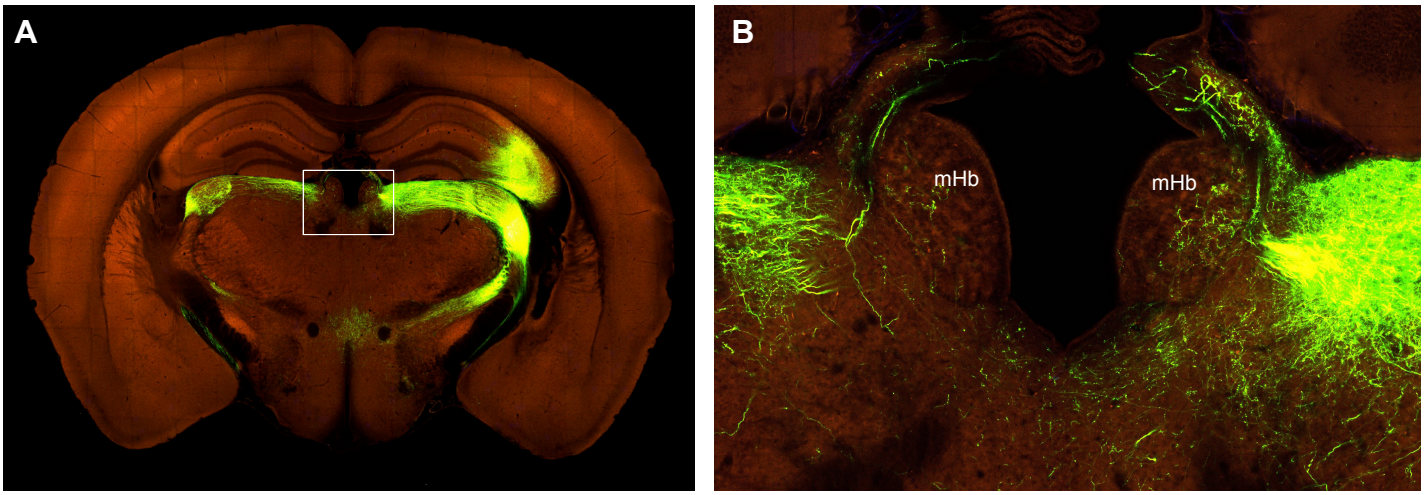

Figure 10. A potential projection from the ventral lateral geniculate nucleus to the habenula in a mouse. Anterograde label was performed by injecting recombinant adeno associated virus into the ventral lateral geniculate nucleus. 0.33 mm^3 was injected into Bregma (-2.46, 2.6, 2.36, 0) of a p56 slc32a1-IRES-Cre mouse, which expresses Cre in GABAergic neurons (Oh et al., 2014). (A) Coronal view, showing an overview of the label. (B) A high magnification of the area boxed in panel A, showing labeled fibers in the habenula. mHb: medial habenula. These images are from http://connectivity.brain-map.org/projection/experiment/siv/267538006?imageId=267538231&imageType=TWO_PHOTON,SEGMENTATION&initImage=TWO_PHOTON&x=14704&y=7847&z=3.